

目錄

(1) 報告內容	2
(1 - 1) 前言	2
(1 - 2) 研究目的	3
(1 - 3) 文獻探討	4
(1 - 4) 研究方法	7
(1 - 5) 結果與討論	8
(1-5-1) System development	9
(1-5-2) application1: poly-thiophene (for polymer solar cell)	22
(1-5-3) application2: azoaromatic dye (for hologram, etc)	32
(2) 參考文獻	43
(3) 計畫成果自評	47

(1) 報告内容

(1 - 1) 前言

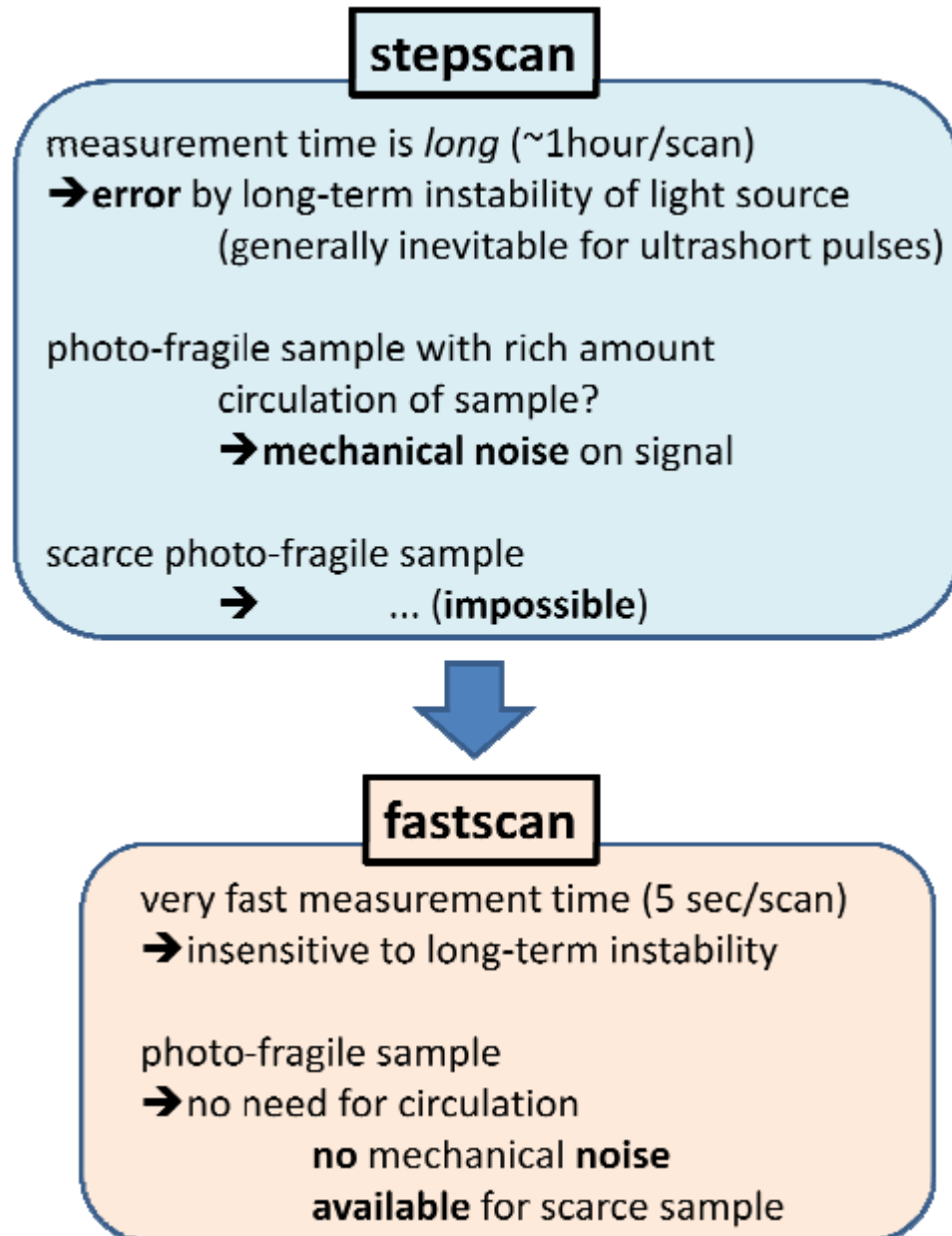


Fig.1 Target of this project

Photochemical reactions are quite useful for human life as explained below. Photosynthesis process in plants provides oxygen for all livings. Photo-isomerization process in rhodopsin (a protein which works as light sensor in eye) is the initial process when a light sensor protein, rhodopsin, catches light on retina of eye. Ultrafast photo processes in materials can be used as a gimmick for optical memory or switch.

Useful photochemical reactions are generally active in visible wavelength region, which can be studied

by ultrashort visible laser pulses generated by non-collinear parametric amplifier (NOPA). Because of its smooth and broad spectrum, the NOPA pulse enabled us to observe ultrafast phenomena in broadband spectral range for the study of probe wavelength dependency of ultrafast dynamics. It helps to clarify **ultrafast dynamics of intermediates in the chemical reaction**. But also, the ultrashort duration of the pulse width makes it possible to time-resolve the motion of molecular vibration. It enables us to study **real-time change of molecular structures of transient states in the photochemical reactions**. After development of **multi-channel lock-in amplifier (MLA) system**, ultrafast dynamics at every probe wavelengths can be measured the lock-in detector arrays in a broad spectral range **in the same time**.

However, one scan of those measurement costs around 1 hour. Therefore, long-term instability of light source contaminates obtained signal seriously, which makes it difficult to obtain reliable data. The other problem caused by long-time measurement period is that the sample is damaged under long-time irradiation by ultrashort laser pulses.

In this project, I plan to develop a fast-scan ultrafast spectroscopy system, which enables us to perform one scan of the ultrafast spectroscopy in several seconds. It is expected to solve above problems being one of the most useful methods for ultrafast spectroscopy.

(1 - 2) 研究目的

In Advanced Laser Research Center (ALRC) of National Chiao-Tung University (NCTU), I have built up a NOPA system to generate sub-10fs visible pulse, which can be used for pump-probe measurement to study ultrafast dynamics of various materials. Multi-channel measurement system was also built up to use together with the ultrashort visible laser pulses. Using both of them, time-resolved measurement can be performed in broadband probe spectral range to study ultrafast dynamics.

However, it is **difficult to obtain reproducible result especially for low frequency modes and quantitative change observed in long time scale** like several hundred femtoseconds. The reason is explained in the following. One scan of pump-probe measurement typically costs almost one hour when we want to observe ultrafast dynamics up to 1 picosecond delay time including information of molecular vibration. **The light pulse intensity of NOPA**, generated by high order nonlinear effect, **can be easily affected by environment** like temperature, humidity, and airflow around the system, even though we are trying to avoid these environmental effects as far as possible. The timescale of the modulation is generally **in the order of minutes**. Even in the current system, we can accurately observe fast signal, like fast decay signal and real-time molecular vibration because NOPA intensity is stabilized in short timescale of seconds by gain saturation in the optical amplification process of NOPA. However, **the instability in timescale of minutes lowers the reproducibility for low frequency modes observed in the signal**.

This project is planned to **develop a fast scan pump-probe system combined with the multi-channel lock-in amplifier (MLA) system**. If one scan of pump-probe measurement can be finished in several seconds (fast scan pump-probe), the observed result can provide **reproducible results even for slow**

dynamics (from 100fs to 10ps). It will provide us **full knowledge about the ultrafast dynamics** of those materials, and help us to elucidate mechanism of ultrafast phenomena in photochemical reactions of various materials. The fast scan pump-probe was never tried with MLA system because of its technical difficulties, and it is a very **challenging project**. The following figure is a preliminary data showing that the fast scan method is expected work well to improve signal-to-noise ratio.

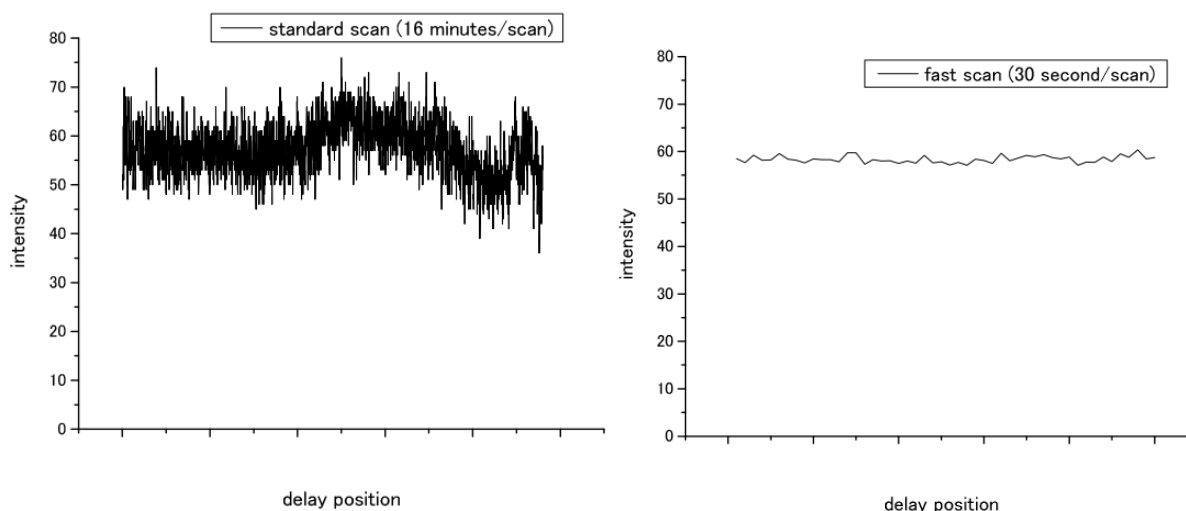


Fig. 2. Intensity instability of NOPA observed in a scan of standard pump-probe measurement, which costs 16 minutes for each scan (left). Estimated intensity instability of NOPA in fast-scan (right). This estimation assumes one scan of fast scan measurement costs 30 seconds and accumulated for many scans during 16 minutes. Long-term instability found in left figure is smoothed out in right figure because of average over many scans of fast-scan.

(1 - 3) 文献探討

Ultrafast spectroscopy is a powerful method for investigating photochemical, photophysical, and photobiological processes. Photochemistry of various reactions has been studied, including isomerization, proton transfer, and electron transfer. Photophysical processes have been measured for carrier dynamics and nonlinear excitations. Photobiological processes have been clarified in vision and photosynthesis [1-3]. Ultrafast spectroscopy also has various important applications to photosensors [4-6], ultrafast optical switches [7-9], and ultrafast optical memories [10-12].

Following the development of femtosecond lasers, ultrafast spectroscopy blossomed [13-16] and expanded into areas such as plasma diagnosis and *in situ* probes for laser manufacturing. Subsequent development of sub-10-fs laser pulses [17-22] elucidated the ultrafast dynamics [23-27] of electronic relaxations and molecular vibrations. After the development of the non-collinear optical parametric amplifier (NOPA) [28-29], ultrafast spectroscopy could be performed across wide spectral regions because its structure is broadband and smooth. The resulting observation of real-time molecular vibrations has provided

information about changes in molecular structure during relaxation processes such as internal conversion and intersystem crossing, and chemical reactions including *cis-trans* and *trans-cis* isomerization, proton transfer, and oxidation [30-37].

However, it has been difficult to obtain reproducible results for molecular vibrational modes across long timescales of several hundred femtoseconds. The difficulty stems mainly from (i) accumulated damage to the samples, and (ii) long-term instabilities in the laser intensity.

In conventional ultrafast pump-probe measurements, the delay time is scanned in fine steps (less than several femtoseconds) across a long time span (up to a few tens of picoseconds) in order to observe molecular vibrational signals along with the electronic dynamics. The relaxation and dynamics of molecular vibrational modes can be studied by observing changes in the instantaneous frequencies of the modes associated with corresponding electronic states. Therefore it is necessary to have both a long time range to follow the reactions and a sufficiently short time step to resolve the molecular vibrations whose frequencies change during the electronic processes. One complete scan can take an hour or more. If the sample is chemically sensitive to radiation, it can be damaged during a single scan. The accumulation of damage, which can be significant when the measurement time is long, makes it difficult to observe the intrinsic dynamics of a sample.

Molecular vibrational periods are on the order of several tens of femtoseconds, observed as a modulation of the ΔA trace in a pump-probe measurement during accumulation of about 100 laser shots at each delay-time step. The intensity of the ultrashort laser pulses, used for generating high order nonlinear effects, is affected by small fluctuations in the temperature, humidity, and airflow around the system. These small disturbances cause instabilities in the laser intensity, which make it difficult to observe the ΔA modulation, because both modulations have roughly the same period of several minutes.

Fast-scan acquisition of the signals could solve these problems by collecting data on the fly and in real time [38]. However, spectroscopic studies require measurement at each probe wavelength. Such iterative measurements are time consuming, and laser damage accumulates on the sample. As a result, the sample condition at the last probe wavelength can be considerably different from that at the first probe wavelength. To overcome that drawback, we have developed a new fast-scan system with multiplex detection. In the present work, we have developed a fast-scan pump-probe system with a multichannel lock-in amplifier (MLA) for multiplex detection. This new method, which we dub "fast-scan pump-probe spectroscopy", improves the reproducibility and reliability of the experimental data. For comparison, conventional pump-probe measurements are first performed for a conjugate polymer film. The data are found to be limited in sensitivity and reliability, because they are affected by instabilities in the light source and by the fragility of the samples. When the pulse duration is kept below 10 fs, which is shorter than typical molecular vibrational periods, it is difficult to maintain the long-term stability of the laser, hindering determination of the decay dynamics of the electronic states and introducing systematic errors. The fragility of the samples reduces the amount and concentration of the samples and can cause contamination of the materials. These effects make it difficult to obtain reproducible and reliable data.

The difficulties are expected to be solved by developing the fast-scan pump-probe spectroscopic

system in this project.

- [1] F. Pellegrino, *Opt. Eng.* **22**, 508 (1983).
- [2] A. B. Rubin, L. B. Rubin, V. Z. Pashchenko, A. A. Kononenko, B. A. Gulyaev, *Kvantovaya Elektron.* **7**, 52 (1980).
- [3] M. R. Wasielewski, P. A. Liddell, D. Barrett, T. A. Moore, D. Gust, *Nature* **322**, 570 (1986).
- [4] A. Boyer, M. Dery, P. Selles, C. Arbour, F. Boucher, *Biosens. Bioelect.* **30**, 415 (1995).
- [5] K. J. Hellingwerf, J. Hendriks, T. Gensch, *J. Biol. Phys.* **28**, 395 (2002).
- [6] Y. Imamoto, M. Kataoka, *Photochem. and Photobiol.* **83**, 40 (2007).
- [7] G. Eichmann, Y. Li, R. R. Alfano, *Opt. Eng.* **25**, 91 (1986).
- [8] D. Hulin, A. Mysyrowicz, Z. Zntonetti, A. Migus, W.T. Masselink, H. Morkoc, H.M. Gibbs, N. Peyghambarian, *App. Phys. Lett.* **49**, 719 (1986)
- [9] C.P. Singh, K.S. Bindra, B. Jain, S.M. Oak, *Opt. Comm.* **245**, 407 (2005).
- [10] L. Kuhnert, *Nature* **319**, 393 (1986).
- [11] S. Tazuke, *Solid Stat. Phys.* **23**, 61 (1988).
- [12] N. E. Korolev, I. Y. Mokienko, A. E. Poletimov, A. S. Shcheulin, *Phys. Solid. Stat.* **127**, **327** (1991).
- [13] A. H. Zewail, *Laser femtochemistry, Science*, **242**, 1645 (1988).
- [14] R. M. Bowman, M. Dantus, A. H. Zewail, *Chem. Phys. Lett.* **156**, 131 (1989).
- [15] M. Gruebele, I. R. Sims, E. D. Potter, A. H. Zewail, *J. Chem. Phys.* **95**, 7763 (1991).
- [16] M. Dantus, A. H. Zewail, *Chem. Rev.* **104**, 1717 (2004).
- [17] A. Baltuska, Z. Wei, M. S. Pshenichnikov, and D. A. Wiersma. *Opt. Lett.* **22**, 102 (1997).
- [18] M. Nisoli, S. De Silvestri, O. Svelto, R. Szipocs, K. Ferencz, Ch. Spielmann, S. Sartania, and F. Krausz., *Opt. Lett.* **22**, 522 (1997).
- [19] A. Shirakawa, I. Sakane, and T. Kobayashi, *Opt. Lett.* **23**, 1292 (1998).
- [20] G. Cerullo, M. Nisoli, S. Stagira, and S. De Silvestri., *Opt. Lett.* **23**, 1283 (1998).
- [21] M. Adachi, K. Yamane, R. Morita, M. Yamashita, *Jpn. J. App. Phys.* **44**, 4123 (2005).
- [22] A. Baltuska, T. Fuji, and T. Kobayashi, *Opt. Lett.* **27**, 306 (2002).
- [23] A. Shirakawa and T. Kobayashi, *Appl. Phys. Lett.* **72**, 147 (1998).
- [24] A. Shirakawa, I. Sakane, M. Takasaka, and T. Kobayashi, *Appl. Phys. Lett.* **74**, 2268 (1999).
- [25] A. Baltuska, M. F. Emde, M. S. Pshenichnikov, and D. A. Wiersma, *J. Phys. Chem. A* **103**, 10065 (1999).
- [26] G. Cerullo, G. Lanzani, M. Muccini, C. Taliani, and S. De Silvestri, *Phys. Rev. Lett.* **83**, 231 (1999).
- [27] R. A. G. Cinelli, V. Tozzini, V. Pellegrini, F. Beltram, G. Cerullo, M. Z.-Rossi, S. D. Silvestri, M. Tyagi, and M. Giacca, *Phys. Rev. Lett.* **86**, 3439 (2001).
- [28] W. T. Pollard, S.-Y. Lee, R. A. Mathies, *J. Chem. Phys.* **92**, 4012 (1990).
- [29] T. Kobayashi, T. Saito, and H. Ohtani, *Nature*, **414**, 531 (2001).
- [30] T. Taneichi, T. Fuji, Y. Yuasa, T. Kobayashi, *Chem. Phys. Lett.* **394**, 377 (2004).
- [31] A. Colonna, A. Yabushita, I. Iwakura, T. Kobayashi, *Chem. Phys.* **341**, 336 (2007).

- [32] A. Yabushita, T. Kobayashi, *Biophys. J.* **96**, 1447 (2009).
- [33] T. Kobayashi, I. Iwakura, A. Yabushita, *New J. Phys.* **10**, 065016 (2008).
- [34] G. Cerullo, G. Lanzani, L. Pallaro, S. De Silvestri, *J. Mol. Struct.* **521**, 261 (2000).
- [35] R. A. G. Cinelli, V. Tozzini, V. Pellegrini, F. Beltram, G. Cerullo, M. Zavelani-Rossi, S. De Silvestri, M. Tyagi, M. Giacca, *Phys. Rev. Lett.* **86**, 3439 (2001).
- [36] T. Cimei, A. R. Bizzarri, G. Cerullo, S. De Silvestri, S. Cannistraro, *Biophys. Chem.* **106**, 221 (2003).
- [37] A. Gambetta, C. Manzoni, E. Menna, M. Meneghetti, G. Cerullo, G. Lanzani, S. Tretiak, A. Piryatinski, A. Saxena, R. L. Martin, A. R. Bishop, *Nature Phys.* **2**, 515 (2006).
- [38] M. J. Feldstein, P. Vohringer, N. F. Scherer, *J. Opt. Soc. Am. B* **12**, 1500 (1995).

(1 - 4) 研究方法

I have already built up the sub-10fs visible pulse and multi-channel lock-in amplifier (MLA) system in the project of Advanced Laser Research Center (ALRC) in National Chiao-Tung University. The project is going to advance in the direction of broader bandwidth generation to develop a measurement system for wider variety of materials that can be investigated with the system. However, during the development in ALRC, I found the instability of light source in long time scale of minutes makes serious problem for analysis of relatively slow dynamics in time range of 100fs to 10ps. To solve this problem, it is necessary to develop a "fast scan" system, which can finish one scan of pump-probe measurements in several seconds. However, the development is quite independent from the direction of the ALRC project. This is the reason why I am applying this project as an independent project. The difficulties in this project are shown in the following together with the possible solutions and schedule.

(1st difficulty: to be solved in the 1st year)

The first difficulty is that a single scan of fast scan measurements should finish in the same time period of several seconds without any delay. During the fast scan on the MLA system, the data cannot be sent to computer to avoid any delay in the scan. The MLA system built in ALRC has memory function. The difficulty can be solved if the fast scan pump-probe data can be stored in the memory. This is planned to be done in the first year of the project by developing software to handle the data storage in the fast scan measurement.

(2nd difficulty: to be solved in the 2nd year)

The second difficulty is that the motorized stage used for standard pump-probe measurement cannot be synchronized well with multi-channel lock-in measurement system, because the stage cannot be synchronized with external trigger signal, which can be used for triggered operation of the lock-in system. Bad synchronization deadens fine time scale signals, like molecular vibration signals observed in

pump-probe signal. The problem of bad synchronization can be solved as follows. In the pump-probe measurement system, we install a fast scan stage, which can be operated by external voltage, and develop an electronic circuit system to scan the fast scan stage synchronized with external trigger signals. Via external trigger signal generated by laser controller, the lock-in system and the fast scan stage can be synchronized well to obtain fine time-resolution even in the fast scan measurement.

(1 – 5) 結果與討論

As a result of this project, I have finished the development of the fast scan system as I planned in the project proposal. The result of fast scan system development has been published as an article in a peer-reviewed scientific journal of "Review of Scientific Instruments". The title of the article is "Development of a multiplex fast-scan system for ultrafast time-resolved spectroscopy" written by Atsushi Yabushita, Yu-Hsien Lee, and Takayoshi Kobayashi. The article was printed in Volume 81, Issue 7 of the journal in 2010. The following shows the result obtained in the work.

The newly developed system was applied for ultrafast spectroscopy of photo-voltaic polymer, P3HT, and the result was published in a peer-reviewed scientific journal of Chemical Physics Letters (Yu Hsien Lee et al, "Ultrafast relaxation dynamics of photoexcitations in poly(3-hexylthiophene) for the determination of the defect concentration", Chem. Phys. Lett. 398, 71-76 (2010)). Using the fastscan ultrafast spectroscopy system, we could get signal of the P3HT film with high signal-to-noise ratio, and estimated the time constant of the relaxation dynamics of bound polaron on the P3HT polymer chains

We also performed ultrafast spectroscopy of Azo dye, DR19, and the result was accepted for publication on a peer-reviewed journal (Chun-Chih Hsu et al, "Environment-Dependent Ultrafast Photoisomerization Dynamics in Azo Dye", The Journal of Physical Chemistry A, dx.doi.org/10.1021/jp2051307, to be published). The dynamics of the DR19 film is hard to be observed because the film can be easily damaged by photo irradiation. The fastscan ultrafast spectroscopy system allowed us to study the ultrafast dynamics of the film because the effect of the photo damage is negligible in each scan of the fast scan finishing in five seconds.

The accomplishment of the development of the fastscan ultrafast spectroscopy system and its applications shows that this project was **accomplished successfully in 100%**.

(1-5-1) System development

Development of a multiplex fast-scan system for ultrafast time-resolved spectroscopy

1. Introduction

Time-resolved studies have been performed using a scanning optical delay line with a motorized stage. They have elucidated the ultrafast dynamics of various materials. In such studies, a lock-in amplifier (LIA) is typically used to improve the signal quality. But an LIA has several problems, including base-band detection and $1/f$ noise, the time required for data acquisition, and modulation of the laser fluence incident on the sample. Fast-scan acquisition of the signals could solve these problems by collecting data on the fly and in real time.¹ However, spectroscopic studies require measurement at each probe wavelength. Such iterative measurements are time consuming, and laser damage accumulates on the sample. As a result, the sample condition at the last probe wavelength can be considerably different from that at the first probe wavelength. To overcome that drawback, we have developed a new fast-scan system with multiplex detection. As an example of the application of this method, we use it to perform femtosecond time-resolved spectroscopy.

Ultrafast spectroscopy is a powerful method for investigating photochemical, photophysical, and photobiological processes. Photochemistry of various reactions has been studied, including isomerization, proton transfer, and electron transfer. Photophysical processes have been measured for carrier dynamics and nonlinear excitations. Photobiological processes have been clarified in vision and photosynthesis.²⁻⁴ Ultrafast spectroscopy also has various important applications to photosensors,⁵⁻⁷ ultrafast optical switches,⁸⁻¹⁰ and ultrafast optical memories.¹¹⁻¹³

Following the development of femtosecond lasers, ultrafast spectroscopy blossomed¹⁴⁻¹⁷ and expanded into areas such as plasma diagnosis and *in situ* probes for laser manufacturing. Subsequent development of sub-10-fs laser pulses¹⁸⁻²³ elucidated the ultrafast dynamics²⁴⁻²⁸ of electronic relaxations and molecular vibrations. After the development of the noncollinear optical parametric amplifier (NOPA),²⁹⁻³⁰ ultrafast spectroscopy could be performed across wide spectral regions because its structure is broadband and smooth. The resulting observation of real-time molecular vibrations has provided information about changes in molecular structure during relaxation processes such as internal conversion and intersystem crossing, and chemical reactions including *cis-trans* and *trans-cis* isomerization, proton transfer, and oxidation.³¹⁻³⁸

However, it has been difficult to obtain reproducible results for molecular vibrational modes across long timescales of several hundred femtoseconds. The difficulty stems mainly from (i) accumulated damage to the samples, and (ii) long-term instabilities in the laser intensity.

In conventional ultrafast pump-probe measurements, the delay time is scanned in fine steps (less than several femtoseconds) across a long time span (up to a few tens of picoseconds) in order to observe molecular vibrational signals along with the electronic dynamics. The relaxation and dynamics of molecular vibrational modes can be studied by observing changes in the instantaneous frequencies of the modes associated with corresponding electronic states. Therefore it is necessary to have both a long time range to follow the reactions and a sufficiently short time step to resolve the molecular vibrations whose frequencies

change during the electronic processes. One complete scan can take an hour or more. If the sample is chemically sensitive to radiation, it can be damaged during a single scan. The accumulation of damage, which can be significant when the measurement time is long, makes it difficult to observe the intrinsic dynamics of a sample.

Molecular vibrational periods are on the order of several tens of femtoseconds, observed as a modulation of the ΔA trace in a pump-probe measurement during accumulation of about 100 laser shots at each delay-time step. The intensity of the ultrashort laser pulses, used for generating high order nonlinear effects, is affected by small fluctuations in the temperature, humidity, and airflow around the system. These small disturbances cause instabilities in the laser intensity, which make it difficult to observe the ΔA modulation, because both modulations have roughly the same period of several minutes.

In the present work, we have developed a fast-scan pump-probe system with a multichannel lock-in amplifier (MLA) for multiplex detection. This new method, which we dub "fast-scan pump-probe spectroscopy", improves the reproducibility and reliability of the experimental data. For comparison, conventional pump-probe measurements are first performed for a conjugate polymer film. The data are found to be limited in sensitivity and reliability, because they are affected by instabilities in the light source and by the fragility of the samples. When the pulse duration is kept below 10 fs, which is shorter than typical molecular vibrational periods, it is difficult to maintain the long-term stability of the laser, hindering determination of the decay dynamics of the electronic states and introducing systematic errors. The fragility of the samples reduces the amount and concentration of the samples and can cause contamination of the materials. These effects make it difficult to obtain reproducible and reliable data. But the experimental data are strikingly improved by using the fast-scan pump-probe spectroscopic system.

2. Experiment

2-1. Noncollinear optical parametric amplifier (NOPA)

We built a noncollinear optical parametric amplifier (NOPA) to generate visible laser light whose spectral width is broad enough to generate sub-10-fs pulses for ultrafast time-resolved spectroscopy. Details of the NOPA are presented in Appendix A. The smooth spectral shape of its output makes it ideal for spectroscopy. The pump source of the NOPA consists of a regenerative chirped pulse amplifier (Legend-USP-HE from Coherent) seeded with a Ti:sapphire laser oscillator (Micra 10 from Coherent). The amplifier generated femtosecond pulses whose duration, central wavelength, repetition rate, and average power were 40 fs, 800 nm, 5 kHz, and 500 mW, respectively. Each pulse from the regenerative amplifier was separated into two pulses by a beam sampler. The larger intensity pulse was used for second harmonic generation centered at 400 nm which pumped the NOPA. The other pulse (with 10 times weaker intensity) was focused onto a sapphire plate to generate white light by self-phase modulation, to be used as a seed beam for the NOPA. The resulting broadband visible output spectrum plotted in Fig. 1 extends from 530 nm ($18\,868\text{ cm}^{-1}$) to 740 nm ($13\,514\text{ cm}^{-1}$) with constant phase. A beamsplitter separated the pump and probe pulses, whose intensities were adjusted using a variable neutral density filter. The energies of the pump and

probe pulses were 1 nJ and 0.2 nJ, respectively. Using a beam compressor consisting of a diffraction grating telescopic dispersion line, multilayer dielectric chirped mirrors, and a computer-controlled flexible mirror, the broadband visible laser pulse was compressed to a 10-fs duration before it arrived at the sample surface. The probe pulse was dispersed by a polychromator (SP2300i from Princeton Instruments) into a fiber bundle, the other end of which was separated into 128 fibers connected to avalanche photodiodes (APDs). The time-resolved transmittance difference ΔT of these 128 probe wavelengths was simultaneously detected. The signals were then sent to a multichannel lock-in amplifier with a high signal-to-noise ratio.

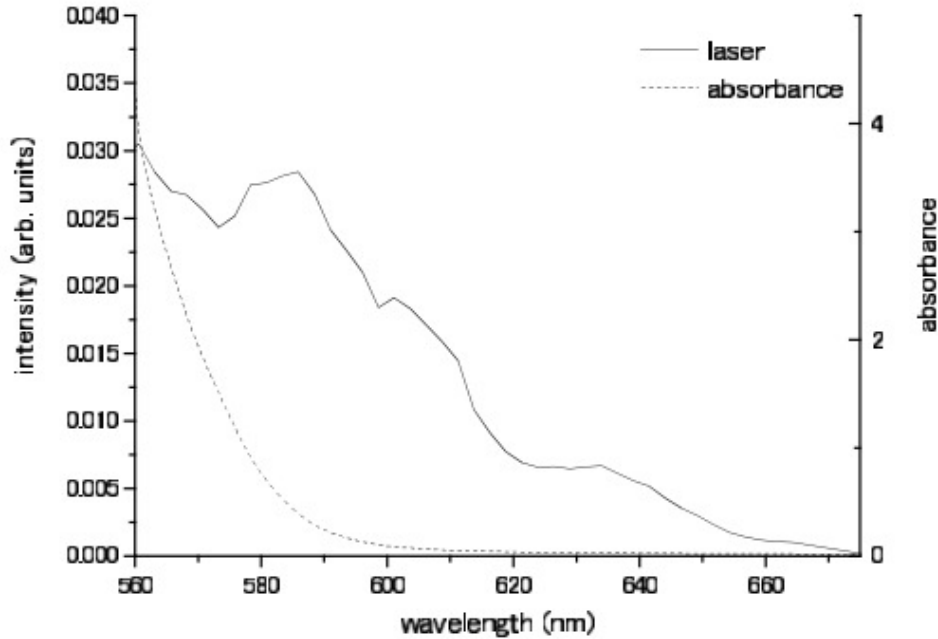


FIG. 1. Incident laser spectrum and absorption spectrum of a sample film.

2-2. Mechanical stage for conventional pump-probe measurements: Step-scan method

To evaluate our new technique, we compared it to a pump-probe signal obtained using a conventional method. A signal was collected by recording ΔA while scanning the delay time between the pump and probe pulses across a range of -300 to 1500 fs in 0.6 -fs steps. For analysis purposes, data with 3 -fs steps were obtained by averaging sets of 5 data points together to suppress artifacts due to interference between the pump and probe pulses. The stage used for the step scan (PFS-1020 from Sigma-Tech) had 10 -nm ($1/15$ -fs) resolution with full closed-loop control. The positioning resolution was sufficient for ultrafast time-resolved spectroscopy, because the time resolution was limited by the duration of the pump and probe pulses. However, the stage required about 600 ms to stabilize between movements, so that a single scan of the pump-probe measurement required at least 30 minutes.

2-3. Mechanical stage for novel pump-probe measurements: Fast-scan method

In our new method, the ΔA signal is recorded while scanning the delay time rapidly in 500 steps across a range of 1790 fs. The fast-scan stage (ScanDelay-15 from APE-Berlin) was controlled by an external voltage

generated by a D/A converter (LPC-361316 from Interface), scanning from -0.2 to $+0.8$ V in 5 s, which is 360 times faster than the 30-min scans of the conventional method. At each delay point, ΔA was obtained in 10 ms, storing the data in the memory of a multichannel lock-in amplifier. Average values were calculated for the data in sets of 24 scans to maintain a good signal-to-noise ratio. Therefore, the measurement time for a single run was 2 minutes (5×24 s). One can thereby avoid laser fluctuations having correlation times longer than that.

3. Results and discussion

The experimental setup, consisting of the NOPA, step-scan stage, and fast-scan stage is shown in Fig. 2(a).

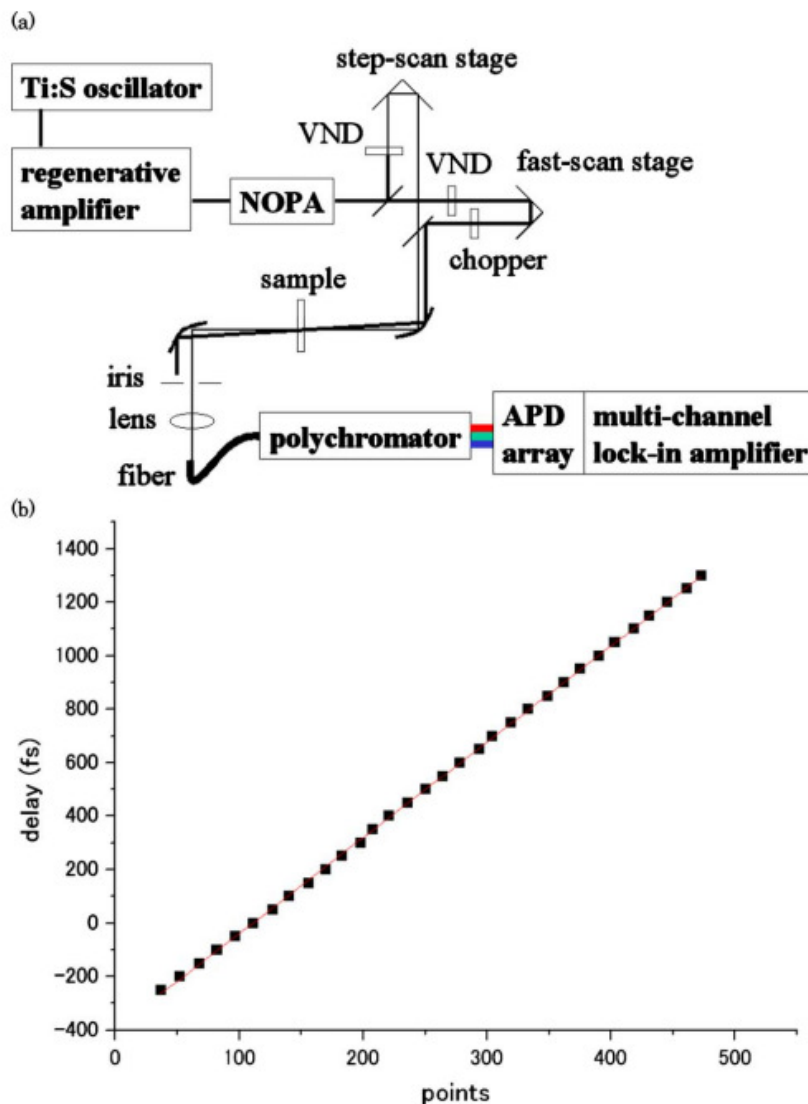


FIG. 2. (Color online) (a) Experimental setup showing the NOPA: noncol-linear optical parametric amplifier, VND: variable neutral density filter, and APD: avalanche photodiode. (b) Calibration data for the fast-scan stage (squares) and a linear fit to the data (solid line).

3-1. Calibration of the delay positions of the fast-scan stage

A 20- μm -thick β -barium borate (BBO) crystal on a fused silica base plate was used to generate an autocorrelation signal from the broadband spectral width of the laser pulse. While scanning the fast-scan stage, the autocorrelation signal was monitored by a photomultiplier tube (H9656-04 from Hamamatsu) connected to the last channel of the MLA system. As the step-scan stage moves, the autocorrelation signal on the fast-scan trace shifts with the same amount of delay. From the shift, the delay position of the fast-scan trace could be calibrated. The autocorrelation traces were obtained by changing the delay position of the step-scan stage in 50-fs steps. The peak positions of the autocorrelation signal are plotted in Fig. 2(b), giving a calibration curve showing a linear relationship between the delay time and data points of 3.58 ± 0.01 fs/point.

3-2. Pump-probe measurements using the step-scan method

Pump-probe measurements of a conjugated polymer film were performed by the step-scan method. The preparation of the sample film is detailed in Appendix B. The absorbance change ΔA in the wavelength region from 515 to 753 nm in 2.5-nm steps was obtained by scanning the delay time from -318 to 1482 fs in 0.6-fs steps (forward scan). For each delay point, ΔA was obtained by accumulating for 0.6 s. The mean ΔA spectra in 3-fs steps are shown in Fig. 3(a) in two-dimensional (2D) form. The data in Fig. 3(b) are for the corresponding backward scan. The poor reproducibility between Figs. 3(a) and (b) is indicative of sample damage and laser intensity instabilities.

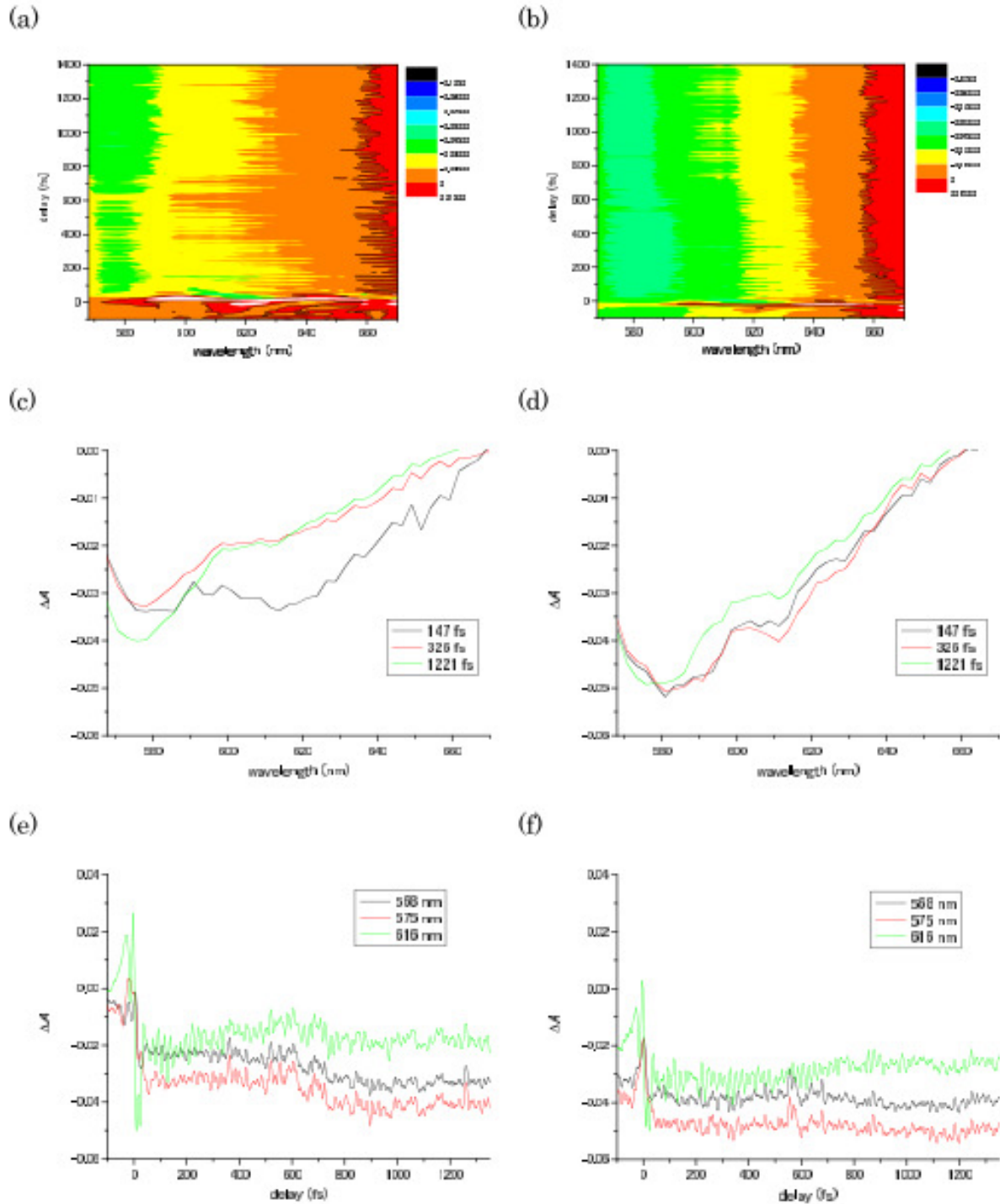


FIG. 3. (Color online) Absorption changes obtained by the step-scan method for delay times of (a) -318 to 1482 fs and (b) 1482 to -318 fs. Time-resolved ΔA spectra at delays of 147 , 326 , and 1221 fs are plotted in (c) and (d), and ΔA traces at 568 , 575 , and 616 nm are plotted in (e) and (f).

The 2D traces give time-resolved ΔA spectra along their cross sections. The ΔA spectra at three delays (147 , 326 , and 1221 fs) are plotted in Figs. 3(c) and (d) for forward and backward scans, respectively. Damage accumulated in the sample causes scattering, which decreases ΔA in panel (d) compared to in panel (c).

Time-resolved ΔA traces at three probe wavelengths (568 , 575 , and 616 nm) were also extracted from

the 2D traces in Figs. 3(a) and (b) and plotted in panels (e) and (f). In the forward scans, the time-resolved traces start around $\Delta A=0$ for negative delays. In contrast, there exists a large offset at negative delays for the backward scans. The offset is due to damage accumulated on the sample during the step-scan measurements.

Fourier power spectra of the ΔA traces reveal molecular vibrational modes of the sample. Figures 4(a) and (b) are the 2D results for forward and backward scans, respectively. They show strong peaks around 1588 cm^{-1} , corresponding to the most intense Raman mode (see Fig. 2 of Ref. 39). However, they have low reproducibility between the forward and backward scans and are not identical in shape with Raman spectra, because of the instability of the laser source.

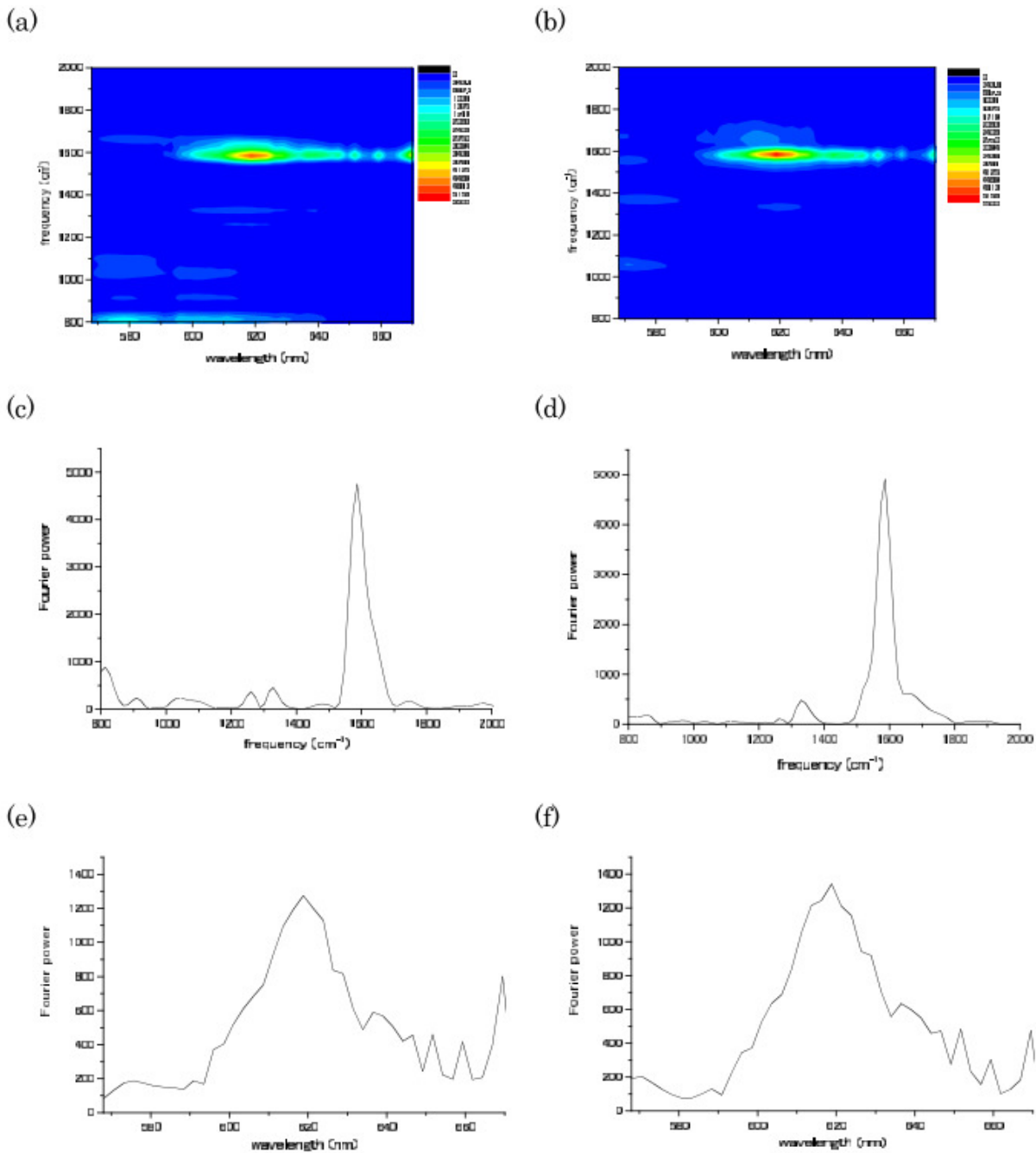


FIG. 4. (Color online) (a) and (b) are Fourier power spectra of the ΔA traces from Figs. 3(a) and 3(b), respectively. Fourier power spectra at 616 nm are plotted in (c) and (d). Fourier power spectra of the most prominent vibrational mode at 1588 cm^{-1} are graphed in (e) and (f).

Fourier power spectra probed at 616 nm were extracted from Figs. 4(a) and (b) and plotted in panels (c) and (d). Irreproducibility of the step-scan data can be seen. Figures 4(e) and (f) are Fourier power spectra of the most prominent mode at 1588 cm^{-1} , corresponding to the C=C stretching mode. They also lack reproducibility.

To study the dynamics of the molecular vibrational modes, a spectrographic analysis was performed. Spectrograms were obtained by a sliding-window Fourier transform using the Blackman window function,

$$S(\omega, \tau) = \int_0^\infty S(t)g(t - \tau)\exp(-i\omega t)dt,$$

$$g(t) = 0.42 - 0.5\cos(2\pi/T) + 0.08\cos(4\pi/T)$$

where τ is the gate width, which we set to 600 fs, corresponding to a FWHM of 240 fs. The calculation of the spectrogram was performed after applying a high-pass filter to the signal, because slow modulations of the signal (slower than tens of femtoseconds) arise from fluctuations in the laser power. For forward and backward scans, the results are shown in Figs. 5(a) and (b), respectively, using a time-resolved ΔA trace probed at 616 nm. They again show poor reproducibility.

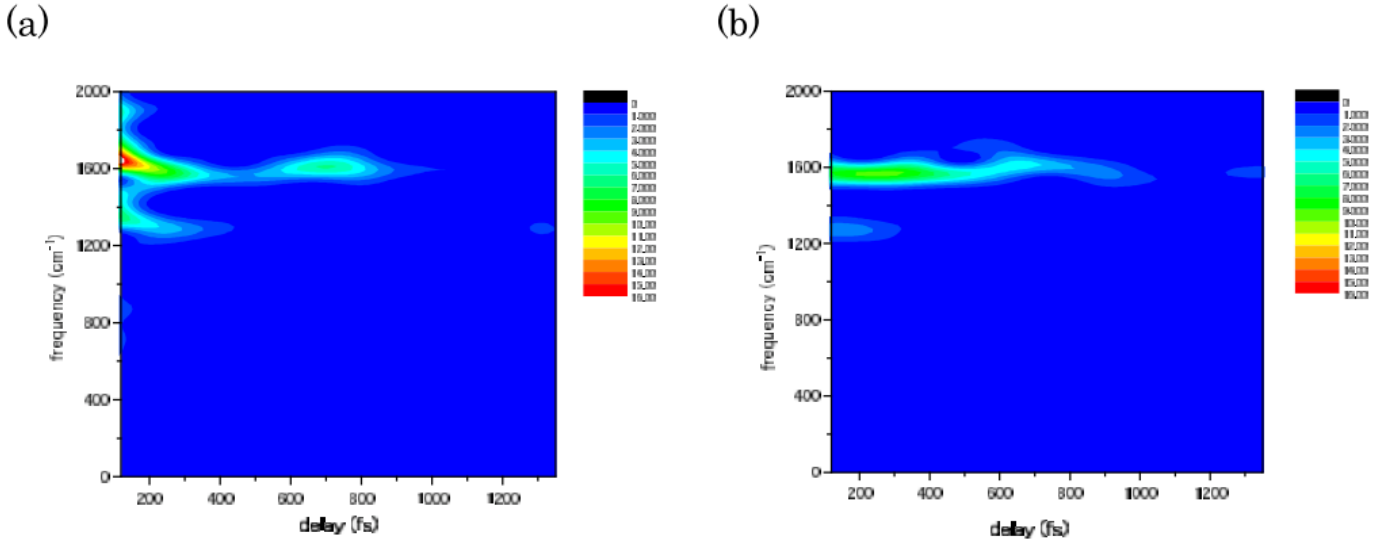


FIG. 5. (Color online) (a) and (b) Spectrograms calculated from the time-resolved traces at 616 nm shown in Figs. 3(e) and 3(f).

3-3. Pump-probe measurements using the fast-scan method

After the preceding step-scan measurements, we moved the sample position to avoid the damaged area and began fast-scan measurements so that the experimental conditions remained identical. Twenty-four forward scans were obtained from -390 to 1396 fs. The mean of the 24 traces is plotted in Fig. 6(a), and backward scanned data from 1396 to -390 fs are shown in Fig. 6(b). In contrast to the step-scan results, these data show high reproducibility.

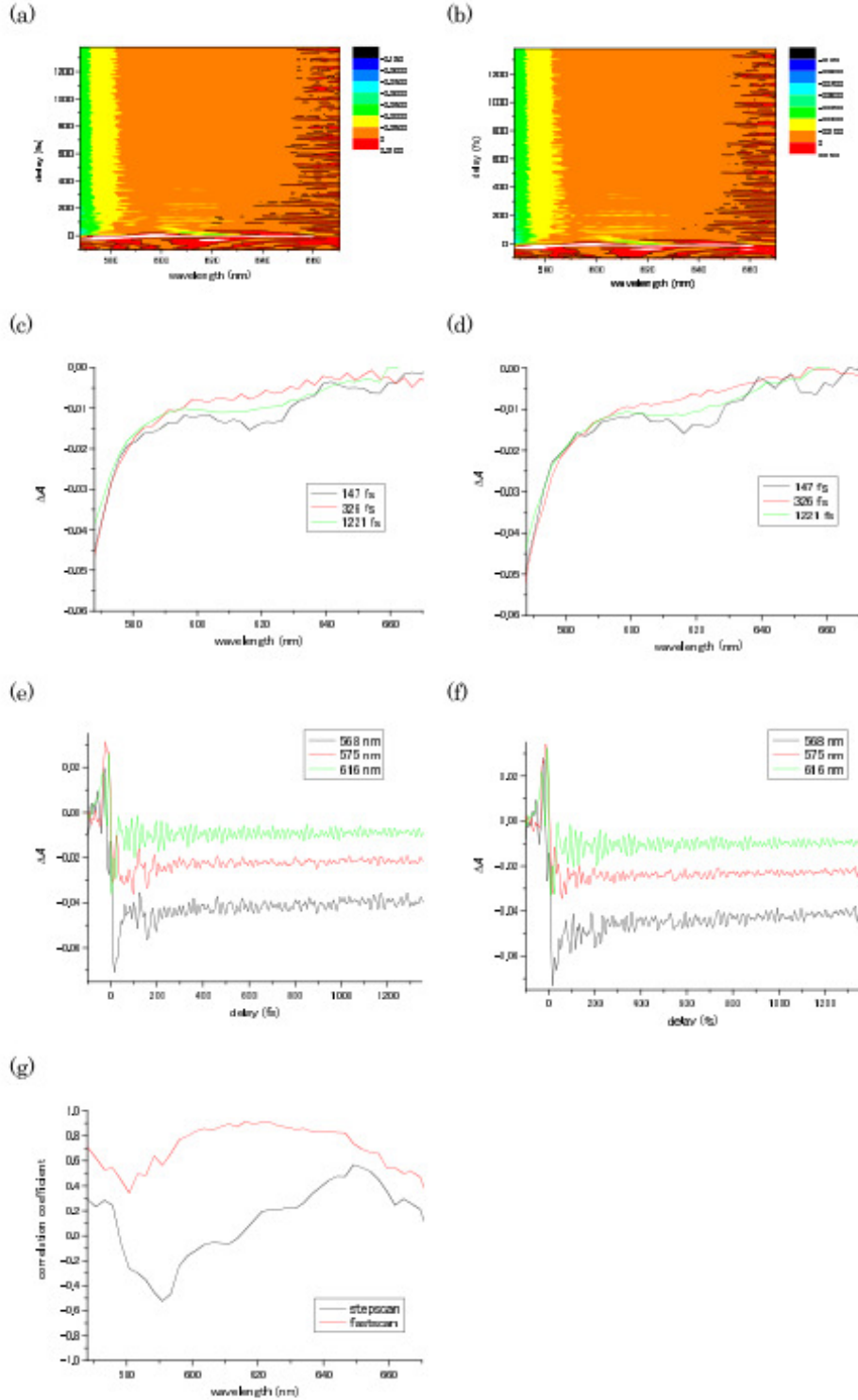


FIG. 6. (Color online) ΔA traces obtained by the fast-scan method for delay times of (a) -390 to 1396 fs, and (b) 1396 to -390 fs. Time-resolved ΔA spectra at delays of 147 , 326 , and 1221 fs are plotted in (c) and (d), and ΔA traces at 568 , 575 , and 616 nm are plotted in (e) and (f). (g) Correlation coefficient between the time traces of the forward and backward scans from 150 to 1350 fs for the step-scan and fast-scan measurements.

Figures 6(c) and (d) are time-resolved ΔA spectra for the forward and backward scans, respectively, at delays of 147 , 326 , and 1221 fs. Time-resolved ΔA traces probed at three wavelengths (568 , 575 , and 616 nm) are plotted for the forward and backward scans in Figs. 6(e) and (f), respectively. The improvement in the signal reproducibility was estimated by calculating a correlation coefficient between the time traces for the

forward and backward scans from 150 to 1350 fs. Figure 6(g) shows the resulting correlation coefficients for the step-scan and fast-scan measurements. One can see that the reproducibility is much higher in the fast-scan measurements than in the step-scan measurements.

Fourier power spectra of the ΔA traces for the forward and backward scans were calculated and are plotted in Figs. 7(a) and (b), respectively. Similar to Figs. 4(c) and (d), ΔA traces probed at 616 nm are plotted in Figs. 7(c) and (d) for forward and backward scans, respectively. They confirm the reproducibility of the Fourier power spectra and show good agreement with Raman spectra from previous work.³⁹ Figures 7(e) and (f) are Fourier power spectra of the most prominent vibrational mode at 1588 cm^{-1} . Some small differences are evident at wavelengths longer than 640 nm. The small amplitude of ΔA in that spectral region [see Figs. 6(a) and (b)] is probably the origin of the error.

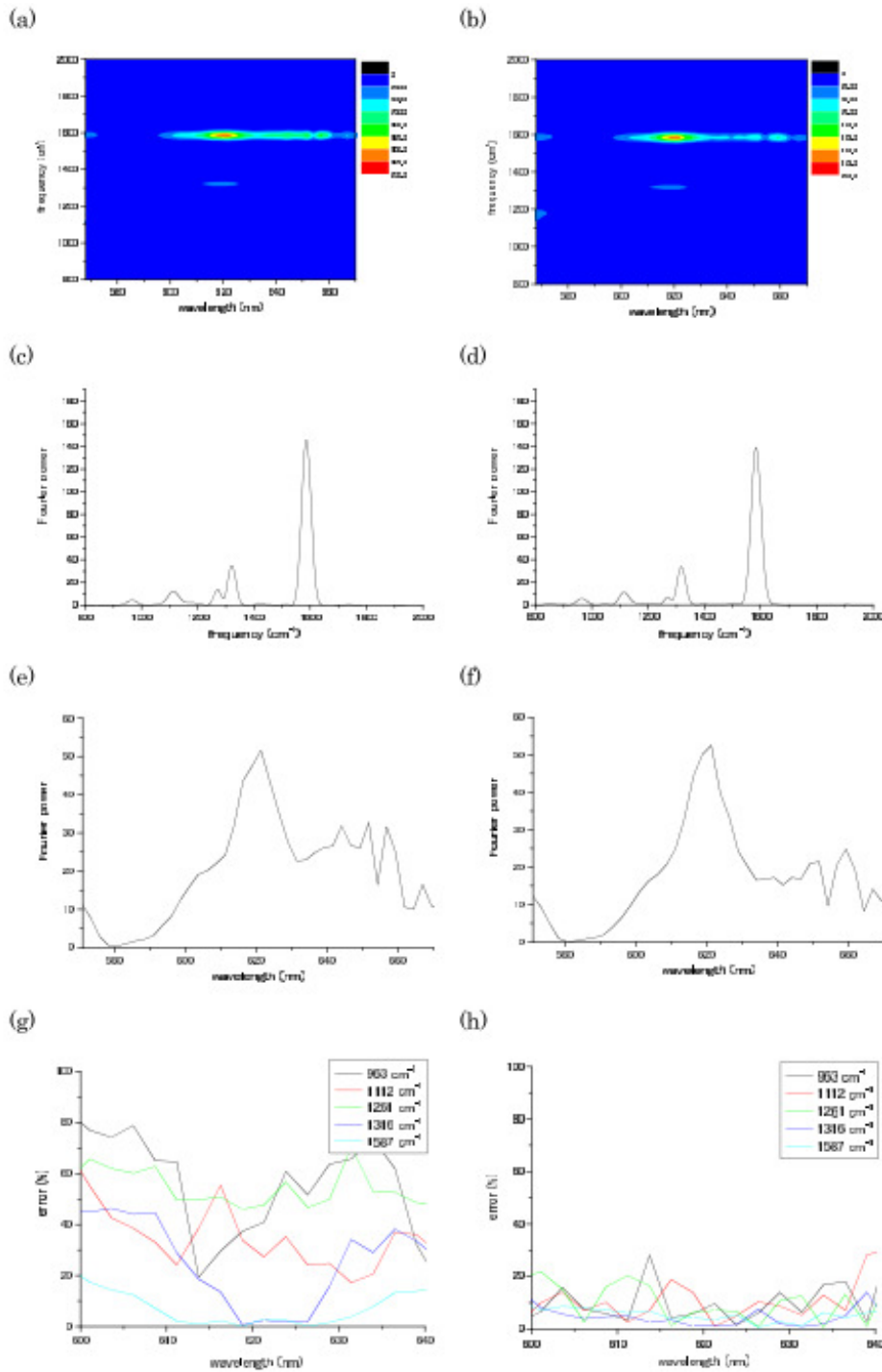


FIG. 7. (Color online) (a) and (b) are Fourier power spectra of the ΔA traces from Figs. 6(a) and 6(b), respectively. Fourier power spectra at 616 nm are plotted in (c) and (d). Fourier power spectra of the most prominent vibrational mode at 1588 cm^{-1} are graphed in (e) and (f). Errors in five vibrational mode intensities for step-scan and fast-scan measurements are shown in (g) and (h).

Between 600 and 640 nm, where the Fourier power is high, the signal reproducibility was quantified by calculating the error in the determination of the power for molecular vibrational modes of 963 , 1112 , 1261 , 1316 , and 1587 cm^{-1} . The relative difference in the Fourier power of a forward scan (I_f) and a backward scan (I_b) is $|(I_f - I_b)/(I_f + I_b)|$. Figures 7(g) and (h) shows the errors calculated for step-scan and fast-scan measurements, respectively. Evidently the Fourier power can be determined more precisely for the latter.

Using a Blackman gate with a FWHM of 240 fs, spectrograms were calculated for the time-resolved traces obtained in the fast-scan measurement. The results are plotted in Figs. 8(a) and (b) for the forward and backward scan, respectively, and show good reproducibility. Therefore, the fast-scan method is preferable not only for the study of electronic dynamics but also for the study of vibrational dynamics.

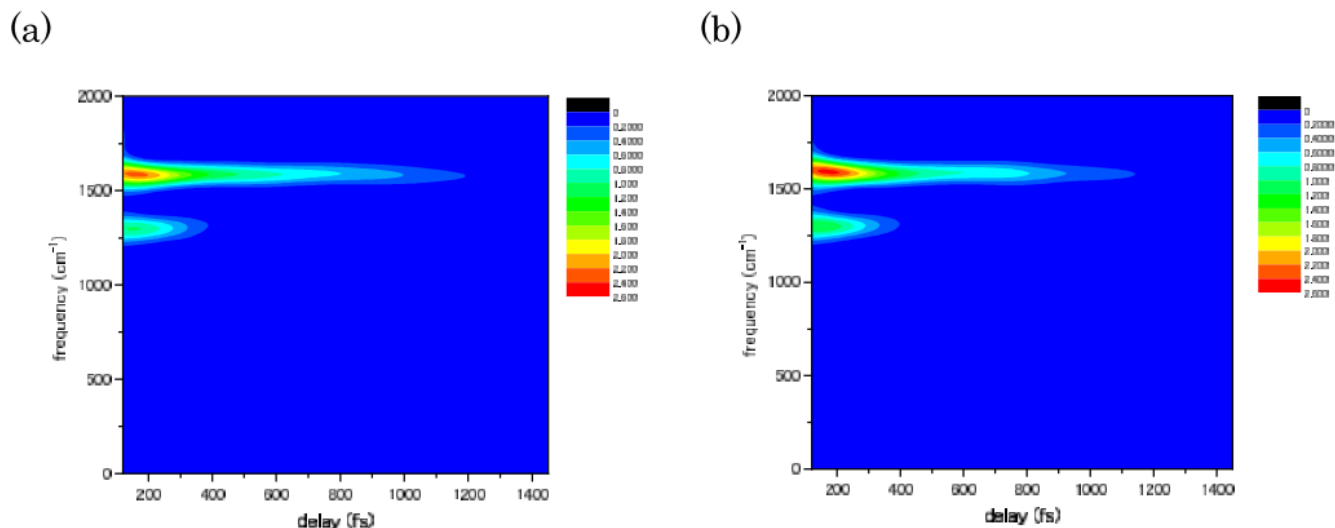


FIG. 8. (Color online) (a) and (b) Spectrograms calculated from the time-resolved ΔA traces at 616 nm plotted in Figs. 6(e) and 6(f).

4. Summary

The fast-scan method obtains time-resolved signals with femtosecond resolution over a picosecond range on the fly and in real time. However, it is traditional in time-resolved spectroscopy to measure data at each probe wavelength one by one, which is time consuming and results in damage accumulation on a sample.

In this paper we reported a new fast-scan system with multiplex detection. It is particularly useful for ultrafast spectroscopy with a fine time resolution. We assessed its advantage over the traditional step-scan method by performing time-resolved spectroscopy using each method. The fast-scan pump-probe system can perform measurements within two minutes. The results show higher reproducibility and reliability than those obtained by the step-scan method.

References

- ¹ M. J. Feldstein, P. Vohringer, N. F. Scherer, *J. Opt. Soc. Am. B* **12**, 1500 (1995).
- ² F. Pellegrino, *Opt. Eng.* **22**, 508 (1983).
- ³ A. B. Rubin, L. B. Rubin, V. Z. Pashchenko, A. A. Kononenko, B. A. Gulyaev, *Kvantovaya Elektron.* **7**, 52 (1980).
- ⁴ M. R. Wasielewski, P. A. Liddell, D. Barrett, T. A. Moore, D. Gust, *Nature* **322**, 570 (1986).
- ⁵ A. Boyer, M. Dery, P. Selles, C. Arbour, F. Boucher, *Biosens. Bioelect.* **30**, 415 (1995).
- ⁶ K. J. Hellingwerf, J. Hendriks, T. Gensch, *J. Biol. Phys.* **28**, 395 (2002).
- ⁷ Y. Imamoto, M. Kataoka, *Photochem. and Photobiol.* **83**, 40 (2007).

- ⁸ G. Eichmann, Y. Li, R. R. Alfano, *Opt. Eng.* **25**, 91 (1986).
- ⁹ D. Hulin, A. Mysyrowicz, Z. Zنونetti, A. Migus, W.T. Masselink, H. Morkoc, H.M. Gibbs, N. Peyghambarian, *App. Phys. Lett.* **49**, 719 (1986)
- ¹⁰ C.P. Singh, K.S. Bindra, B. Jain, S.M. Oak, *Opt. Comm.* **245**, 407 (2005).
- ¹¹ L. Kuhnert, *Nature* **319**, 393 (1986).
- ¹² S. Tazuke, *Solid Stat. Phys.* **23**, 61 (1988).
- ¹³ N. E. Korolev, I. Y. Mokienko, A. E. Poletimov, A. S. Shcheulin, *Phys. Solid. Stat.* **127**, **327** (1991).
- ¹⁴ A. H. Zewail, *Laser femtochemistry, Science*, **242**, 1645 (1988).
- ¹⁵ R. M. Bowman, M. Dantus, A. H. Zewail, *Chem. Phys. Lett.* **156**, 131 (1989).
- ¹⁶ M. Gruebele, I. R. Sims, E. D. Potter, A. H. Zewail, *J. Chem. Phys.* **95**, 7763 (1991).
- ¹⁷ M. Dantus, A. H. Zewail, *Chem. Rev.* **104**, 1717 (2004).
- ¹⁸ A. Baltuska, Z. Wei, M. S. Pshenichnikov, and D. A. Wiersma. *Opt. Lett.* **22**, 102 (1997).
- ¹⁹ M. Nisoli, S. De Silvestri, O. Svelto, R. Szipocs, K. Ferencz, Ch. Spielmann, S. Sartania, and F. Krausz., *Opt. Lett.* **22**, 522 (1997).
- ²⁰ A. Shirakawa, I. Sakane, and T. Kobayashi, *Opt. Lett.* **23**, 1292 (1998).
- ²¹ G. Cerullo, M. Nisoli, S. Stagira, and S. De Silvestri., *Opt. Lett.* **23**, 1283 (1998).
- ²² M. Adachi, K. Yamane, R. Morita, M. Yamashita, *Jpn. J. App. Phys.* **44**, 4123 (2005).
- ²³ A. Baltuska, T. Fuji, and T. Kobayashi, *Opt. Lett.* **27**, 306 (2002).
- ²⁴ A. Shirakawa and T. Kobayashi, *Appl. Phys. Lett.* **72**, 147 (1998).
- ²⁵ A. Shirakawa, I. Sakane, M. Takasaka, and T. Kobayashi, *Appl. Phys. Lett.* **74**, 2268 (1999).
- ²⁶ A. Baltuska, M. F. Emde, M. S. Pshenichnikov, and D. A. Wiersma, *J. Phys. Chem. A* **103**, 10065 (1999).
- ²⁷ G. Cerullo, G. Lanzani, M. Muccini, C. Taliani, and S. De Silvestri, *Phys. Rev. Lett.* **83**, 231 (1999).
- ²⁸ R. A. G. Cinelli, V. Tozzini, V. Pellegrini, F. Beltram, G. Cerullo, M. Z.-Rossi, S. D. Silvestri, M. Tyagi, and M. Giacca, *Phys. Rev. Lett.* **86**, 3439 (2001).
- ²⁹ W. T. Pollard, S.-Y. Lee, R. A. Mathies, *J. Chem. Phys.* **92**, 4012 (1990).
- ³⁰ T. Kobayashi, T. Saito, and H. Ohtani, *Nature*, **414**, 531 (2001).
- ³¹ T. Taneichi, T. Fuji, Y. Yuasa, T. Kobayashi, *Chem. Phys. Lett.* **394**, 377 (2004).
- ³² A. Colonna, A. Yabushita, I. Iwakura, T. Kobayashi, *Chem. Phys.* **341**, 336 (2007).
- ³³ A. Yabushita, T. Kobayashi, *Biophys. J.* **96**, 1447 (2009).
- ³⁴ T. Kobayashi, I. Iwakura, A. Yabushita, *New J. Phys.* **10**, 065016 (2008).
- ³⁵ G. Cerullo, G. Lanzani, L. Pallaro, S. De Silvestri, *J. Mol. Struct.* **521**, 261 (2000).
- ³⁶ R. A. G. Cinelli, V. Tozzini, V. Pellegrini, F. Beltram, G. Cerullo, M. Zavelani-Rossi, S. De Silvestri, M. Tyagi, M. Giacca, *Phys. Rev. Lett.* **86**, 3439 (2001).
- ³⁷ T. Cimei, A. R. Bizzarri, G. Cerullo, S. De Silvestri, S. Cannistraro, *Biophys. Chem.* **106**, 221 (2003).
- ³⁸ A. Gambetta, C. Manzoni, E. Menna, M. Meneghetti, G. Cerullo, G. Lanzani, S. Tretiak, A. Piryatinski, A. Saxena, R. L. Martin, A. R. Bishop, *Nature Phys.* **2**, 515 (2006).
- ³⁹ T. P. Nguyen, S. H. Yang, P. Le Rendu, H. Khan, 2005, *Composites A* **36**, 515 (2005).

(1-5-2) application1: poly-thiophene (for polymer solar cell)

Ultrafast relaxation dynamics of photoexcitations in poly(3-hexylthiophene) for the determination of the defect concentration

1. Introduction

Conjugated polymers have been studied extensively because they have peculiar properties, including plasticity and semiconductivity, that make them attractive for use in large-area devices for electro-optical and optoelectronic applications [1-8]. As one example of an electro-optical application, considerable progress has been made in developing electroluminescent devices based on poly(arylenevinylene) [9,10]. As one example of an optoelectronic application, organic solar cells that use conjugated-polymer-based compounds have recently been studied widely since they are expected to become a low-cost replacement for conventional silicon photovoltaics. Polymer-based solar cells have many advantages over conventional solar cells, including low toxicity, adjustable electronic and mechanical properties, and ease of fabrication. The energy conversion efficiency of a solar cell based on a bulk heterojunction consisting of a polymer donor of regioregular poly(3-hexylthiophene) (P3HT) and an acceptor of [6,6]-phenyl-C61-butyric acid methyl ester was reported to be 4.4% [11]. The dynamic of charge carriers contribution in P3HT was recently studied by Randy J. Ellingson group [12], using THz pulses to probe the picosecond relaxation of P3HT, and the basic schematic of interchain transfer was also illustrated from the basis of previous works with the formation and relaxation of bound polaron pairs. However, due to the limited time-resolution of the measurement, ultrafast formation and relaxation of BPP could not be time-resolved by the THz system.

In this present study, we studied the ultrafast dynamics of P3HT using sub-10-fs visible laser pulse. The ultrafast time-resolution enabled us to determine the time constants of 90 ± 2 fs and 710 ± 40 fs, which correspond to formation and relaxation, respectively, of a bound polaron pair (BPP). Defect concentration on P3HT was also estimated observing pump intensity dependence of the signal.

2. Experiment

2.1. Non-Collinear Optical Parametric Amplifier

We have constructed a non-collinear optical parametric amplifier (NOPA) to generate visible laser pulses, whose spectral width is sufficiently broad to support sub-10 fs visible pulses useful for ultrafast time-resolved spectroscopy [13-15]. The smooth spectral shape of the NOPA output is suitable for time-resolved spectral measurements. A regenerative chirped pulse amplifier (Legend-USP-HE; Coherent) seeded with a Ti:sapphire laser oscillator (Micra 10; Coherent) was used to pump and seed the NOPA. The amplifier generates 40-fs pulses with a central wavelength of 800 nm, a repetition rate of 5 kHz, and an average power of 2.5 W. The beam from the regenerative amplifier is split into two beams by a beam sampler. One beam had a power of 800 mW and it was used to generate a second harmonic with a wavelength of 400 nm that was employed to pump the NOPA. The other beam had a power of 2.5 mW and was focused on a sapphire plate to induce self-phase modulation to generate white light, which is used as the seed beam of the

NOPA. The NOPA generates a broad visible spectrum extending from 520 to 700 nm with a nearly constant phase (see Fig. 1). A beam splitter splits the visible laser pulse into pump and probe beams. The intensities of the pump and probe beams are adjusted using a variable neutral density filter and the ratio of the pump intensity to the probe intensity is set to be about four for the weakest excitation. The duration of the broadband visible laser pulse is compressed to 9 fs using a pulse compression system, which consists of a diffraction-grating telescopic dispersion line, specially designed multilayer dielectric chirped mirrors, and a computer-controlled flexible mirror. The probe pulse is dispersed by a polychromator (SP2300i; Princeton Instruments) into a 128-branch fiber bundle, whose other end is separated into 128 fiber branches and connected to avalanche photodiodes (APDs). Therefore, the time-resolved transmittance differences ΔT at 128 probe wavelengths are simultaneously detected at the APDs. The signals detected at the APDs are sent to a multichannel lock-in amplifier developed by our group to obtain a signal with a high signal-to-noise ratio.

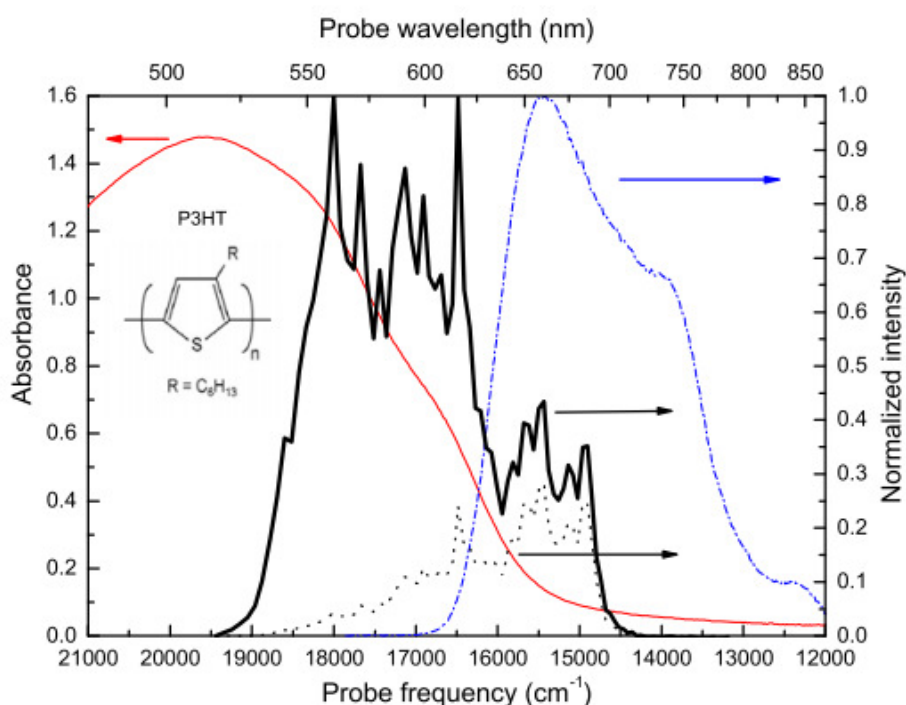


Figure 1. Stationary absorption spectrum (thin solid curve), laser spectrum (thick solid curve), transmittance spectrum (dotted curve), and fluorescence spectrum (dashed curve). The inset shows the molecular structure of P3HT.

2.2. Materials

Highly regioregular poly(3-hexylthiophene) (*P3HT*) (P200; Rieke Metals, Inc.) was purchased and used without further treatment. The sample has HT(head-to-tail)-HT ratio >98 % and average molecular weight of 50,000. It was dissolved in 1,2-dichlorobenzene (15 mg/mL) stirring at 50 °C for 12 hours to ensure complete dissolution. A P3HT thin film was formed by dip-coating on one surface of a glass substrate (25×25×0.5 mm³) to be used as a sample in this work. Figure 1 shows the stationary absorption spectrum of the formed P3HT film recorded using an ultraviolet–visible–near-infrared scanning spectrophotometer

(UV-3101PC; Shimadzu). Figure 1 also shows a photoluminescence spectrum measured by an ARC SpectraPro-150 luminescence spectrometer equipped with a deuterium lamp as the excitation light source. All measurements were performed at room temperature (295 ± 1 K).

3. Results and discussion

3.1 Time-resolved difference absorption spectra

Pump-probe measurements of P3HT films were performed to obtain time-resolved difference absorption spectra ($\Delta A(\lambda, t)$) in the wavelength range 530 to 680 nm in 2.5 nm steps; the scanning delay time was varied from -350 to 1400 fs in 3.6 fs steps. Figure 2(a) shows the observed two-dimensional (2D) ΔA spectrum and Fig. 2(b) shows ΔA traces at eight probe wavelengths. The time traces contain exponential decay reflecting electronic dynamics and oscillation reflecting vibration dynamics. In the following sections, we have performed exponential fitting to elucidate the ultrafast dynamics of the P3HT after photoexcitation. Analysis on the vibration dynamics is going to be studied in future work.

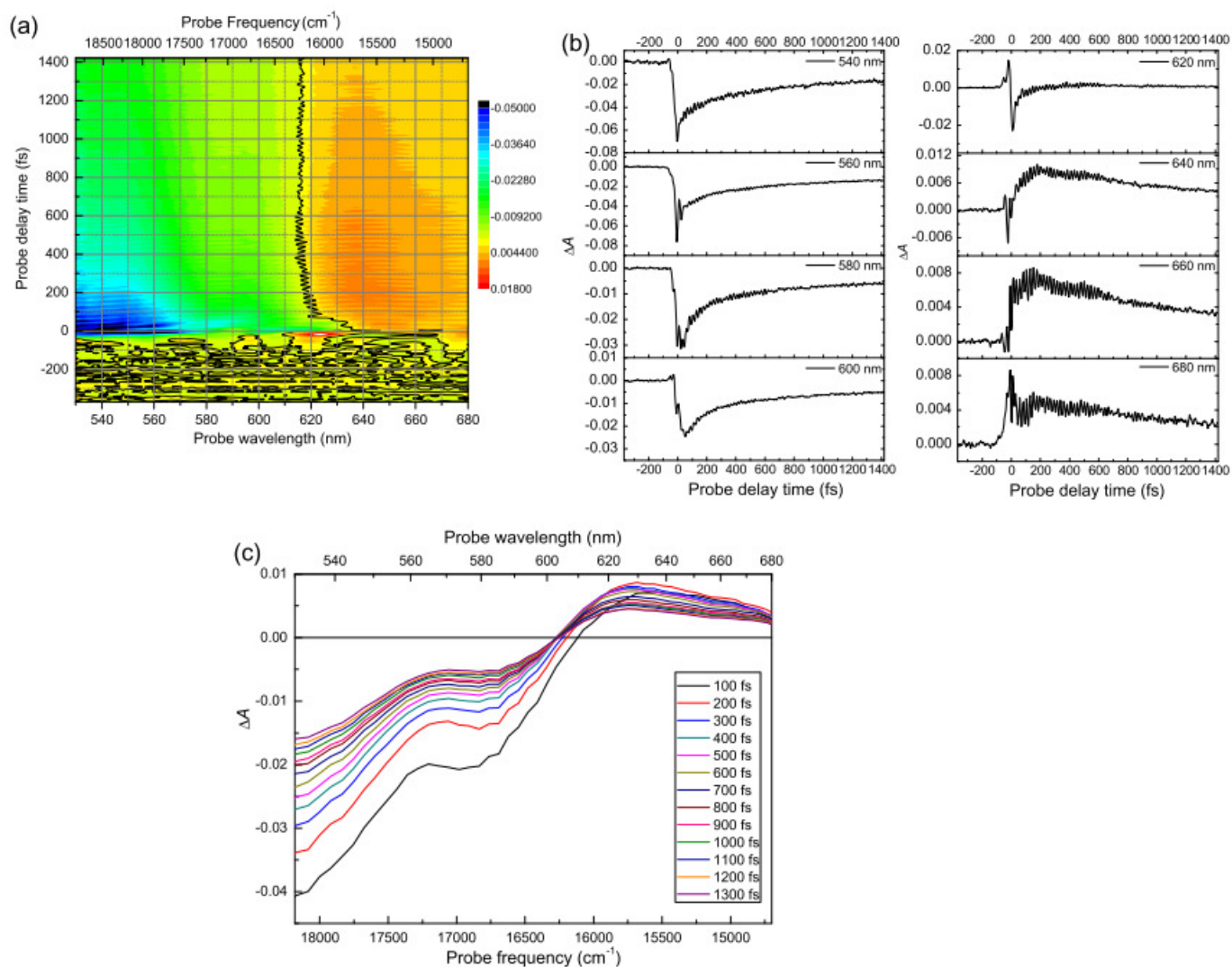
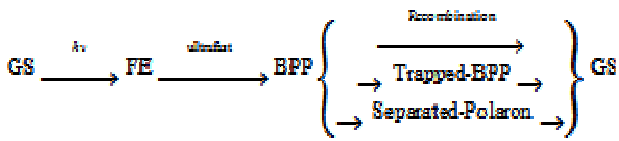


Figure 2. (a) Two-dimensional display of the time dependence of the absorbance changes (probe photon energy versus probe delay time). The value of ΔA is shown by a pseudocolor, and the curve represents the probe photon energy where $\Delta A = 0$. (b) Pump-probe delay time dependence of the difference absorbance probed at eight different wavelengths. (c) Time-resolved ΔA spectra averaged over 100 fs.

The difference absorbance, ΔA , is negative at short wavelengths and becomes positive at wavelengths longer than about 610 nm. The positive ΔA signal is due to induced absorption in transitions from the first electronic excited state to higher states. Stimulated emission from the excited state and photobleaching due to ground-state (GS) depletion could be the origins of the negative ΔA signal. The photobleaching has a much longer lifetime than stimulated emission because stimulated emission occurs only from the excited singlet exciton state, whereas photobleaching occurs until the GS has been fully repopulated. Figure 2(c) shows the time-resolved absorbance change spectra averaged for 100 fs, which clearly indicates the existence of ultrafast decay in the spectral region shorter than 610 nm.

3.2 Estimation of time constants

Previous study shows that photo-excited P3HT proceeds the following processes [12]:



Here, FE is a free exciton, which undergoes a fast geometrical relaxation to form a BPP (equivalent to a self-trapped exciton). This generated BPP then relaxes to the GS via the three parallel processes of "recombination", "trapping by defect states", and "dissociation into a positive carrier and a negative carrier (polarons)". From the stationary absorption spectrum of the sample and laser spectrum shown in Fig. 1(a), we could estimate how many photons of a single laser pulse were absorbed by the P3HT sample, which is equal to the number of FEs formed by photoexcitation. When the pump power was 10.8 nJ, the FE density was calculated to be $1.8 \times 10^{19} \text{ cm}^{-3}$. Using the calculated FE density and the reported rate constant γ for exciton–exciton annihilation (EEA) in P3HT ($4.0 \times 10^{-9} \text{ cm}^3 \text{ s}^{-1}$) [21], the mean flight time before EEA was estimated to be 14 ps, which is considerably longer than the measured delay time region of 1.5 ps. Therefore, the effect of EEA on the formation dynamics of BPPs from FEs was not considered here.

To determine time constants of above processes, the real-time traces of $\Delta A(\lambda, t)$ in the time region between 60 and 1400 fs were fitted with the sum of two exponential functions and a constant term. The fitting result determined the two time constants, t_1 and t_2 , as shown in Fig. 3(a). In the longer wavelength region (from 620 to 680 nm), the ultrafast decay of ΔA is not prominent compared with that at wavelengths shorter than 620 nm, which is why the time constants could not be determined by the fitting in the longer wavelength region of Fig. 3(a). Global fitting was performed for the observed time-resolved 2D- ΔA trace to determine the time constants precisely (see Fig. 3(b)). The mean square errors were calculated by varying the lifetimes in a stepwise manner to determine the condition for the least square error (LSE). The results for three scans gave $t_1 = 90 \pm 2 \text{ fs}$ and $t_2 = 710 \pm 40 \text{ fs}$.

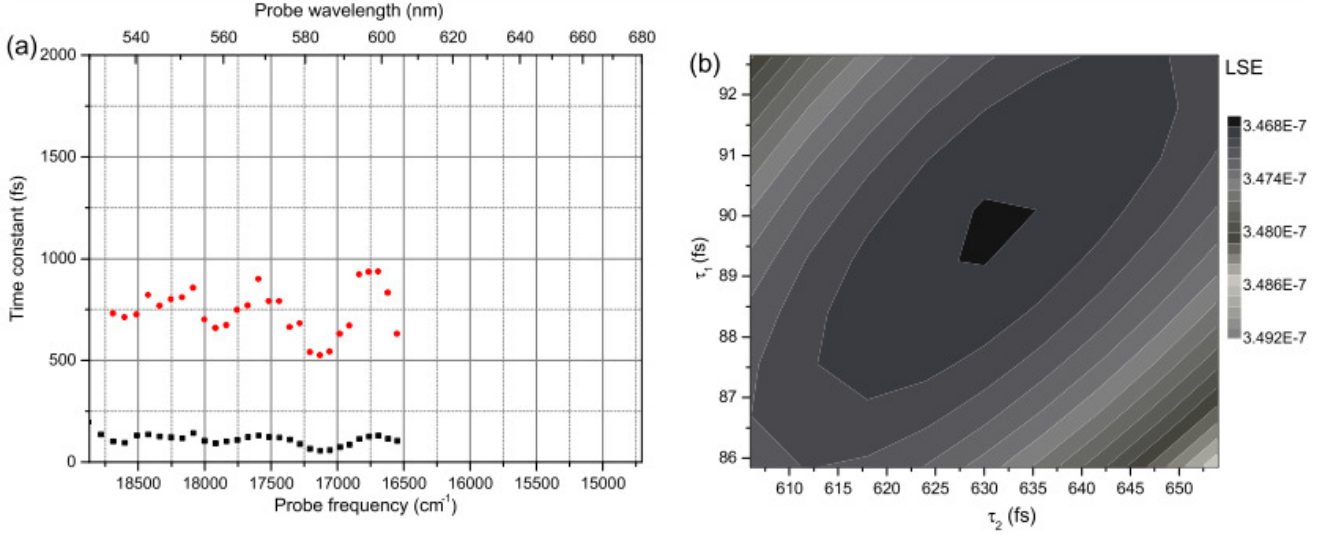


Figure 3. Time constants obtained by a calculation using a two-exponential fit performed for ΔA traces in (a) short delay region (from -0.35 to 1.4 ps) and (b) global fitting results for ΔA traces by the method of least-squares.

The obtained values of t_1 and t_2 could be respectively assigned to the formation and decay of a BPP, as were assigned to a self-trapped exciton in previous works [16-18]. Self-trapped excitons only occur in one-dimensional systems being equivalent to bound polaron pairs (BPPs) [12,19,20]. Previous study estimated the formation time constant of a BPP as shorter than 100 fs, but it was not time-resolved [17]. As seen above, the formation time constant of the BPP was firstly time-resolved in this work as 90 ± 2 fs.

3.3 Spectra of the intermediates

Using the obtained time constants of t_1 and t_2 , time-resolved absorption change spectra $\Delta A(\lambda, t)$ was fitted by double exponential function of

$$\Delta A(\lambda, t) = b_1(\lambda) e^{-\frac{t}{t_1}} + b_2(\lambda) e^{-\frac{t}{t_2}} + b_0(\lambda) \quad (t_1 < t_2) \quad (1)$$

in the time range from 60 to 1400 fs and the wavelength range from 550 to 600 nm applying the LSE method. As explained in the following, $b_0(\lambda)$, $b_1(\lambda)$, and $b_2(\lambda)$ obtained in the fitting can be used to calculate $b_{FE}(\lambda)$ and $b_{BPP}(\lambda)$, which represent contribution from FE and BPP, respectively.

Photo-excitation of P3HT generates FE, which makes transition to BPP in t_{FE} . The BPP relaxes in parallel three processes of "recombination", "trapping", and "dissociation". The whole processes can be expressed by the following equation,

$$\Delta A(\lambda, t) = b_{FE}(\lambda) e^{-\frac{t}{t_{FE}}} + b_{BPP}(\lambda) \left(1 - e^{-\frac{t}{t_{FE}}} \right) e^{-\frac{t}{t_{BPP}}} + b_{RBPP}(\lambda) \left(1 - e^{-\frac{t}{t_{FE}}} \right) \left(1 - e^{-\frac{t}{t_{BPP}}} \right), \quad (2)$$

where suffixes FE and BPP correspond to a free exciton and a bound polaron pair. The last term of RBPP stands for relaxed BPP made of trapped BPP and separated polaron, whose lifetimes are much longer than the time region studied in this work. For simplicity of calculation, single time constant of t_{BPP} represents contributions of three parallel decay processes of BPP, which were decomposed by studying pump power dependence in section 3.5.

In previous section, t_1 (90 ± 2 fs) and t_2 (710 ± 40 fs) were assigned to the formation and decay of BPP, which correspond to t_{FE} and t_{BPP} of Eq. (2). Therefore, considering the relation of $t_{FE} \ll t_{BPP}$, Eq. (2) can be approximated as

$$\Delta A(\lambda, t) = b_{FE}(\lambda)e^{-\frac{t}{t_{FE}}} + b_{BPP}(\lambda)\left(e^{-\frac{t}{t_{BPP}}} - e^{-\frac{t}{t_{FE}}}\right) + b_{RBPP}(\lambda)\left(1 - e^{-\frac{t}{t_{BPP}}}\right). \quad (3)$$

Using equations (1) and (3), we obtain

$$b_1(\lambda) = b_{FE}(\lambda) - b_{BPP}(\lambda),$$

$$b_2(\lambda) = b_{BPP}(\lambda) - b_{RBPP}(\lambda),$$

$$b_0(\lambda) = b_{RBPP}(\lambda).$$

These three equations give

$$b_{BPP}(\lambda) = b_2(\lambda) + b_0(\lambda),$$

$$b_{FE}(\lambda) = b_1(\lambda) + b_2(\lambda) + b_0(\lambda).$$

Using the two relations, $b_{FE}(\lambda)$ and $b_{BPP}(\lambda)$ can be calculated from $b_0(\lambda)$, $b_1(\lambda)$ and $b_2(\lambda)$ obtained in the double exponential fit. The calculated $b_{FE}(\lambda)$ and $b_{BPP}(\lambda)$ are shown in Fig. 4(a).

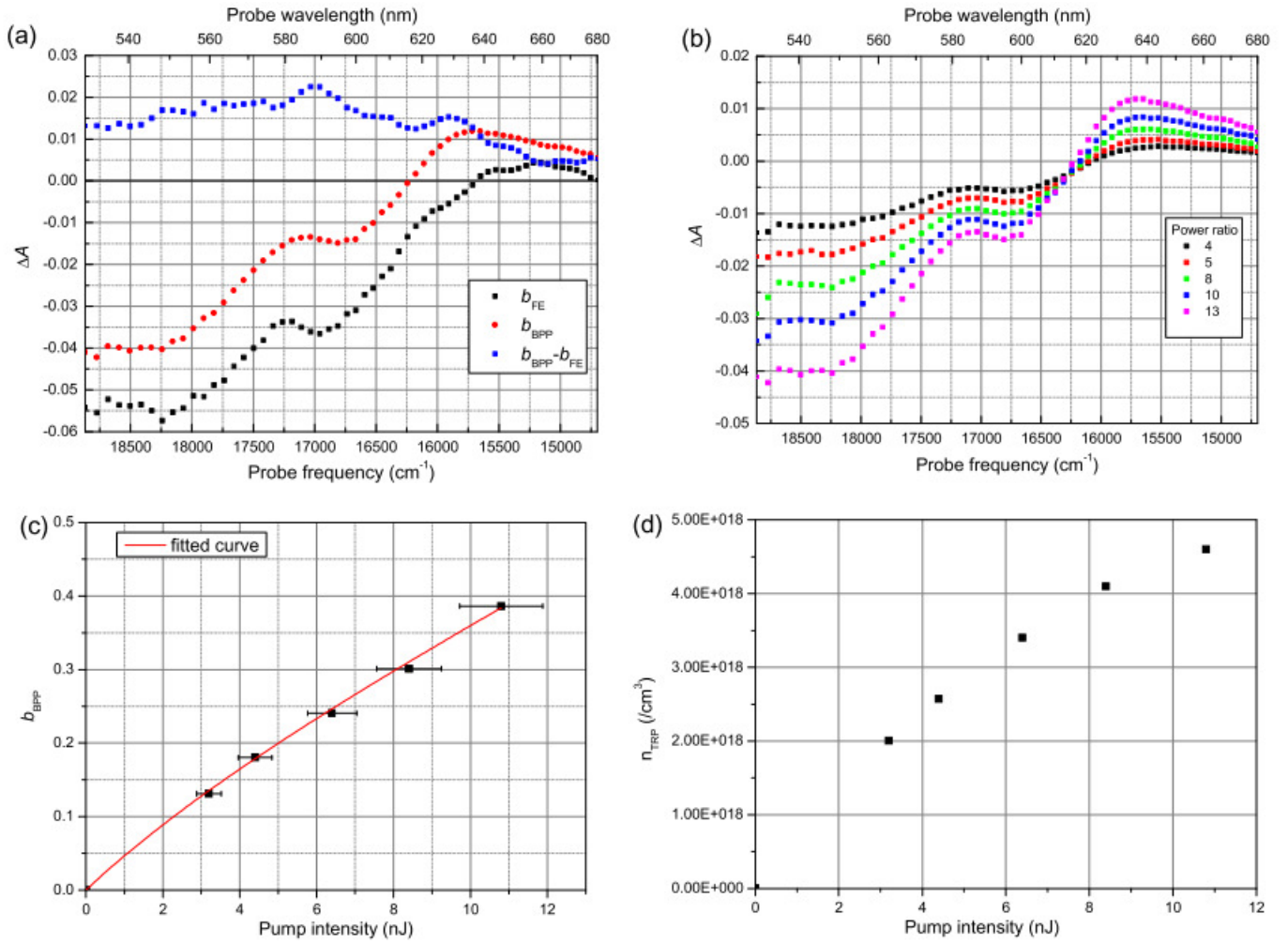


Figure 4. (a) Difference absorption spectra corresponding to ultrafast decaying free-excitons minus the ground-state (b_{FE}), sub-picosecond decaying bound polaron pairs minus the ground-state (b_{BPP}), and the difference between b_{BPP} and b_{FE} , which reflects induced absorption of bound polaron pairs ($b_{BPP} - b_{FE}$). (b) Pump intensity dependence of b_{BPP} . (c) Fitting curve for b_{BPP} observed at different pump intensities. (d) Density of trapped BPP at different pump intensity.

3.4 Defect concentration studied by pump power dependence

The b_{FE} term reflects the transition from a FE to a BPP [12,20]. b_{FE} is negative showing spectral structure similar with that of stationary absorption spectrum in the spectral range from 530 to 630 nm, therefore it is thought to be due to photobleaching as a result of GS depletion. The spectrum of the second component b_{BPP} corresponds to the spectrum of BPP state, which follows relaxation induced by "recombination returning to the GS", "trapping by defects", and "dissociation into a positive carrier and a negative carrier (polarons)" [12]. The spectral structure of b_{BPP} in the probe wavelength region shorter than 610 nm is similar with that of b_{FE} , showing the contribution of photo-bleaching. Subtracting b_{FE} (contribution of photo-bleaching) from b_{BPP} , positive ΔA component was obtained as shown in Fig. 4(a), which reflects the induced absorption spectrum of BPP. In Eq. (3), the last term is a long lifetime component, being beyond our measurement time range, is attributed to the decay of BPPs including the delocalization of charge carriers along the polymer chain [12].

As discussed above, b_{BPP} is composed of three parallel relaxation components of recombination ($b_{\text{BPP,REC}}$), defect trapping ($b_{\text{BPP,TRP}}$), and dissociation ($b_{\text{BPP,DIS}}$). $b_{\text{BPP,TRP}}$ is thought to be independent of the pump intensity when the pump intensity is sufficiently high to cause the trapping process to saturate due to the finite number of traps. In contrast, $b_{\text{BPP,REC}}$ and $b_{\text{BPP,DIS}}$ are proportional to the pump intensity since no saturation effects are expected in the recombination and dissociation processes. Therefore, the coefficient of the second component when the $b_{\text{BPP,TRP}}$ absorption is saturated resulting in homogeneous broadening is given by:

$$b_{\text{BPP}}(I) = b_{\text{BPP,TRP}} + (b_{\text{BPP,REC}} + b_{\text{BPP,DIS}}) = C_1 \frac{I}{1+I/I_s} + C_2 I \quad (4)$$

where I and I_s are the pump intensity and the saturation pump intensity, respectively. C_1 and C_2 are the fitting parameters. Therefore, $b_{\text{BPP,TRP}}$ can be separated from $b_{\text{BPP,REC}}+b_{\text{BPP,DIS}}$ if we perform pump-probe measurements varying the pump intensity.

Figure 4(b) shows b_{BPP} obtained by varying the pump intensity. The pump pulse energy was set to 3.2, 4.4, 6.4, 8.4, and 10.8 nJ, while the probe pulse energy was fixed at 0.9 nJ. We investigated the dependence of the area of the b_{BPP} spectrum between 550 and 600 nm on the pump power, and we estimated the ratio of $C_1:C_2$. In Fig. 4(c), the pump power dependency of b_{BPP} integrated over the spectral range is plotted with a fitting curve fitted by the function shown in Eq. (4). From the fitting result, I_s was estimated to be 7 ± 3 nJ and $C_1:C_2$ was calculated to be $0.46\pm 0.02:0.53\pm 0.05$.

The number of trapped BPPs (n_{TRP}) in P3HT can be determined by

$$n_{\text{TRP}} = \frac{C_1 \frac{I}{1+I/I_s}}{C_1 \frac{I}{1+I/I_s} + C_2 I} P \quad (6)$$

where P is the number of absorbed photons and Fig. 4(d) shows the observed pump power dependency of the number of the trapped BPPs. The limit of the number of trapped BPPs as I approaches infinity gives the number of defect sites on P3HT, and the defect concentration was estimated to be $1.2\times 10^{19} \text{ cm}^{-3}$.

A previous study found that a lamellar structure is formed on P3HT thin films [22], resulting in a lower relaxation energy for interchain charge transfer than that for one-dimensional chains. When all the BPPs (i.e., self-trapped excitons) have undergone interchain transfer, they have the possibility to be trapped by the defect sites. We estimated the volume of a single chain of P3HT to be $3.95\times 10^{-20} \text{ cm}^3$ by a Monte Carlo method. Based on the defect concentration and the volume of P3HT chains, we estimate that on average about two defect sites are present in the volume occupied by three P3HT chains in this sample. This indicates an interesting conclusion that the generated BPPs are not trapped at the end of the main chain but are reflected back from the ends.

3.5 Decomposition of parallel decay rates of BPP

Here, the time constants of defect trapping, recombination, and dissociation of BPP were estimated as follows. The ultrafast growth and fast relaxation are respectively expressed by τ_{GR} and τ_{BPP} assuming that they obey the following relationships:

$$\tau_{GR} = \frac{1}{\kappa_{FE \rightarrow BPP}} \quad (7)$$

$$\tau_{BPP} = \frac{1}{\kappa_{TRP} + \kappa_{DIS} + \kappa_{REC}} \quad (8)$$

where κ_i ($i=FE \rightarrow BPP$, TRP, DIS, REC) represents the rate constants for formation, defect trapping, dissociation, and recombination of BPP.

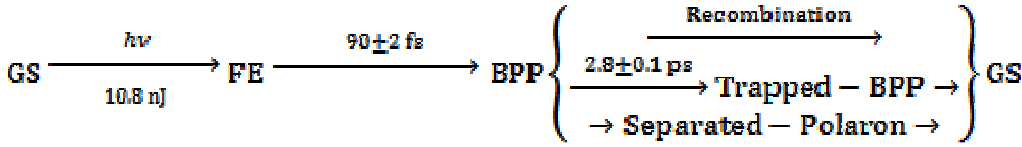
The ratios between the parallel decay processes of BPP are given as

$$\eta_i = \frac{\kappa_i}{\kappa_{TRP} + \kappa_{DIS} + \kappa_{REC}} \quad (9)$$

where i is TRP, DIS, REC. From the above study of pump power dependency, we can determine that

$$\kappa_{TRP} = \frac{\eta_{TRP}}{\tau_{BPP}}, \text{ and } \kappa_{DIS} + \kappa_{REC} = \frac{(\eta_{DIS} + \eta_{REC})}{\tau_{BPP}} = \frac{(1 - \eta_{TRP})}{\tau_{BPP}}$$

Under the highest excitation (10.8 nJ) the ratio between TRP and REC+DIS was determined to be 1:3 by Eq. (4) showing that the 710 ± 40 fs decay of BPPs consists of a 2.8 ± 0.1 ps relaxation caused by defect trapping and a 0.95 ± 0.05 ps relaxation caused by recombination and dissociation into positive and negative carriers (polarons). Therefore, the reactions of P3HT after photoexcitation in the highest excitation case can be summarized as follows.



4. Conclusions

A pump-probe measurement of a P3HT thin film was performed using 9-fs laser pulses. Due to the extremely high temporal resolution of these measurements, the time constant for the formation of BPPs (which previously had been known to be approximately 100 fs) was accurately measured to be 90 ± 2 fs and the time constant for BPP decay was measured to be 710 ± 40 fs (see Fig. 3). The ultrafast time-resolved absorbance change (ΔA) traces were simultaneously measured at 128 probe wavelengths over broadband visible spectral region. The observed 2D- ΔA data was decomposed by LSE analysis to obtain the ΔA spectrum related to FE and BPP. The pump power dependency was used to determine the number of trapped BPPs, whose maximum value reflects the number of defect sites on P3HT. The obtained result clarified that the concentration of defects (which trap BPPs) in the P3HT film is $1.2 \times 10^{19} \text{ cm}^{-3}$. Based on this estimation, we concluded that two out of three main chains has a defect and that the chain ends do not trap BPPs.

References

- [1] T. Blythe, D. Bloor, Electrical Properties of Polymers, Cambridge University Press, Cambridge, 2002.

- [2] C. Brabec, V. Dyakonov, J. Parisi, N.S. Sariciftci, Springer, Berlin, 2003.
- [3] R.H. Friend, R.W. Gymer, A.B. Holmes, J.H. Burroughes, R.N. Marks, C. Taliani, D.D.C. Bradley, D.A. Dos Santos, J.L. Brédas, M. Lögdlund, W.R. Salaneck, *Nature* 397 (1999) 121.
- [4] N. Tessler, G.J. Denton, R.H. Friend, *Nature* 382 (1996) 695.
- [5] G. Hadziioannou, P.F.V. Hutten, *Semiconducting Polymers*, Wiley-VCH, Weinheim, 2000.
- [6] A. Kohler, D.A. Dos Santos, D. Beljonne, Z. Shuai, K.L. Bredas, A.B. Holmes, A. Kraus, K. Mullen, R.H. Friend, *Nature* 392 (1998) 903.
- [7] B.J. Schwartz, *Annu. Rev. Phys. Chem.* 54 (2003) 141.
- [8] E. Hendry, J.M. Schins, L.P. Candeias, L.D.A. Siebbeles, M. Bonn, *Phys. Rev. Lett.* 92 (2004) 196601.
- [9] J.M. Kang, M.J. Park, S.K. Kim, C. Lee, S.H. Jin, D.H. Hwang, *Curr. Appl. Phys.* 6 (2006) 756.
- [10] D.H. Hwang, J.M. Kang, J.H. Eom, M.J. Park, H.J. Cho, J.I. Lee, H.Y. Chu, C. Lee, S.H. Jin, H.K. Shim, *Curr. Appl. Phys.* 9 (2009) 441.
- [11] G. Li, V. Shrotriya, J.S. Huang, Y. Yao, T. Moriarty, K. Emery, Y. Yang, *Nat. Mater.* 4 (2005) 864.
- [12] X. Ai, M.C. Beard, K.P. Knutsen, S.E. Shaheen, G. Rumbles, R.J. Ellingson, *J. Phys. Chem. B* 110 (2006) 25462.
- [13] A. Shirakawa, I. Sakane, T. Kobayashi, *Opt. Lett.* 23 (1998) 1292.
- [14] A. Shirakawa, I. Sakane, M. Takasaka, T. Kobayashi, *Appl. Phys. Lett.* 74(16) (1999) 2268.
- [15] A. Baltuska, T. Fuji, T. Kobayashi, *Opt. Lett.* 27 (2002) 306.
- [16] T. Kobayashi, M. Yoshizawa, U. Stamm, M. Taiji, M. Hasegawa, *J. Opt. Soc. Am. B* 7 8 (1990) 1558.
- [17] T. Kobayashi, *Syn. Met.* 71 (1995) 1663.
- [18] A. Matsuse, S. Takeuchi, K. Yoshino, T. Kobayashi, *Chem. Phys. Lett.* 288 (1998) 165.
- [19] B. Kraabel, D. McBranch, N.S. Sariciftci, D. Moses, A.J. Heeger, *Phys. Rev. B* 50 (1994) 18543.
- [20] A. Ruseckas, M. Theander, M.R. Andersson, M. Svensson, M. Prato, O. Inganäs, V. Sundström, *Chem. Phys. Lett.* 322 (2000) 136.
- [21] P.E. Shaw, A. Ruseckas, I.D.W. Samuel, *Adv. Mater.* 20 (2008) 3516.
- [22] H. Sirringhaus, P.J. Brown, R.H. Friend, M.M. Nielsen, K. Bechgaard, B.M.W. Langeveld-Voss, A.J.H. Spiering, R.A.J. Janssen, E.W. Meijer, P. Herwig, D.M. de Leeuw, *Nature* 401 (1999) 685.

(1-5-3) application2: azoaromatic dye (for hologram, etc)

Environment-Dependent Ultrafast Photoisomerization Dynamics in Azo Dye

1. Introduction

Over the past decades, trans-cis photoisomerization has been one of the most widely investigated photochromic reactions. Azoaromatic dyes [1] are typical systems that exhibit trans-cis photoisomerization. They have been extensively investigated and various experimental techniques have been used to clarify the trans-cis photoisomerization mechanism [2-4]. Irradiation by linearly polarized light results in reversible trans-cis-trans isomerization via a hole-burning mechanism. This isomerization reorientates the molecules, causing the dye to become birefringent by making the azobenzene groups sensitive to optical polarization [5]. Thus, azoaromatic dyes can be used in various applications such as dynamic volume holograms [6,7], waveguide media [8], and light-driven molecular scissors [9]. To improve their performance, it is essential to elucidate the ultrafast dynamics of the photoisomerization process. There have been several recent studies of the ultrafast dynamics of azobenzene dyes; for example, Koller et al. [10] used infrared spectroscopy to investigate 4-nitro-4-(dimethylamino)azobenzene and Poprawa-Smoluch et al. [11] used absorption spectroscopy to study Disperse Red 1. Disperse Red 19 (DR19) is a commercial azobenzene nonlinear optical chromophore with a large ground-state dipole moment of 8 Debye [12-13]. In the present report, we investigate the ultrafast dynamics of solution and film samples of DR19 using absorbance difference spectroscopy with a femtosecond time resolution.

2. Experiments

The azobenzene dye DR19 (dye content 95%) was purchased from Sigma-Aldrich Co. and used after recrystallization. A solution sample was prepared by dissolving 0.1 wt% DR19 in trimethylolpropane triglycidyl ether (TMTE; technical grade; Sigma-Aldrich). A polymer film sample of DR19 was prepared as follows. 0.1 wt% DR19 was dissolved in TMTE and a harden agent (1,2-diaminopropane). The solution was cast on a flat glass (doctor-Blade method) [14] to form a polymer film. The polymer film was estimated to have an average thickness of 0.5 mm by a slide caliper.

The solution and film samples were respectively stored in a sealed vial and a dry box in a dark-adaptive ambient until immediately prior to being used. Figure 1 shows stationary absorption spectrum of the solution and film samples. The absorption peaks at 494 and 500 nm for the solution and film samples, respectively, are due to the strongly allowed π - π^* transition [15].

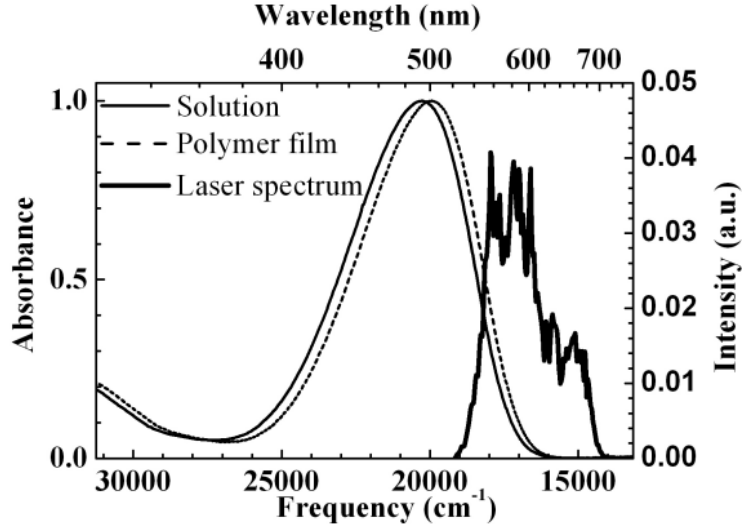


Figure 1: Normalized absorption spectra of DR19 in solution (solid line) and a polymer film (dashed line). The spectrum of NOPA output (thick solid line) used for both pump and probe pulses.

Time-resolved spectroscopy of the samples was performed using ultrashort visible pulses generated by a noncollinear optical parametric amplifier [16,17] seeded by a 5-kHz regenerative Ti:sapphire amplifier (Coherent Inc. Legend-USP-HE). These ultrashort visible pulses had a broad spectrum that extended from 514 to 758 nm (see Fig. 1). The instrument response time was adjusted to be 9 fs by monitoring the pulse width using second-harmonic-generation frequency-resolved optical gating (SHG-FROG) measurements [18] (see below).

In the pump-probe measurements of the solution sample, the pulse width was compressed to 9 fs in a 1-mm glass cell as follows. We first inserted a 1-mm-thick glass plate in front of the entrance of the SHG-FROG system and adjusted pulse compressor to obtain 9 fs pulses. It set the pulse width to be 9 fs after passing through the 1-mm-thick glass. The glass walls of the glass cell used for the solution measurement have the same thickness of 1 mm. If the 1-mm-thick glass is removed and the pulse comes into the glass cell, the pulse width becomes 9 fs inside the glass cell passing through one side of the 1-mm-thick glass wall.

In the pump-probe measurements of the film sample, the pulse width was also adjusted to 9 fs without inserting any glass plate. Therefore, the instrument response time was 9 fs in both cases. The pump beam was focused to a $1.4 \times 10^{-5} \text{ cm}^2$ spot. The pump and probe pulse energies were 8 nJ and 0.8 nJ, respectively.

The probe pulse intensity at each probe wavelength was simultaneously detected by Si avalanche photodiodes attached to a monochromator (Princeton Instruments, SpectraPro 2300i). A mechanical chopper was inserted in the optical path of the pump pulse and was operated at a frequency of 2.5 kHz so that it was in synchronization with the laser pulses. Changes in the transmitted intensity of the probe pulse induced by the pump pulse were processed by a 96-channel lock-in amplifier referenced to the frequency and phase of the chopper. Preamplifiers were used to amplify the electric current measured by the avalanche photodiodes prior to lock-in detection. Because the preamplifier had a cut-off frequency of 5 kHz, harmonic noise of the 2.5

kHz reference frequency was not detected in the observed signals.

For time-resolved spectroscopy of the solution sample, the sample was placed in a 1-mm-thick quartz flow cell (Starna Cells Inc., 48-Q-1; flow rate: 50 ml/min) and was recirculated by a peristaltic pump to ensure that each laser pulse irradiated a fresh sample. To prevent the photogenerated cis isomer accumulating during measurements, the peristaltic pump was connected to a reservoir containing a large volume (60 ml) of the solution sample. During time-resolved measurements of the absorbance difference of the polymer film sample, the position of the sample was changed after each scan to ensure that photodamage did not accumulate during the measurement. Each scan of the time-resolved absorption difference spectra was performed in 5 seconds using a multiplex fast-scan system [19]. In the data analysis, we used data averaged over 40 scans. When the sample was irradiated at the same position for half an hour, the sample was damaged and caused strong scattering light. Meanwhile, the photodamage was negligible in the scan time of 5 seconds.

In the present measurement, the beam diameter on the sample is about 20 micrometers, which is about ten times larger than the period of the optically inscribed grating reported by Barrett et al. [20]. Therefore, the sample still exists inside the beam spot even after the irradiation.

All experiments were performed at room temperature.

3. Results and discussion

3.1 Ultrafast dynamics of the solution sample

Figure 2(a) shows a two-dimensional plot of absorbance difference (ΔA) spectrum of the DR19 solution sample measured for delays from -0.1 to 1.4 ps (short delay region) and probe wavelength from 514 to 758 nm. Figure 2(b) shows the ΔA spectrum measured between -1 and 14 ps (long delay region) in the same probe wavelength region. The black curves in Figs. 2(a) and (b) are contours for which ΔA is zero. Figures 2(c) and (d) show ΔA traces for five different probe wavelengths in Figs. 2(a) and (b).

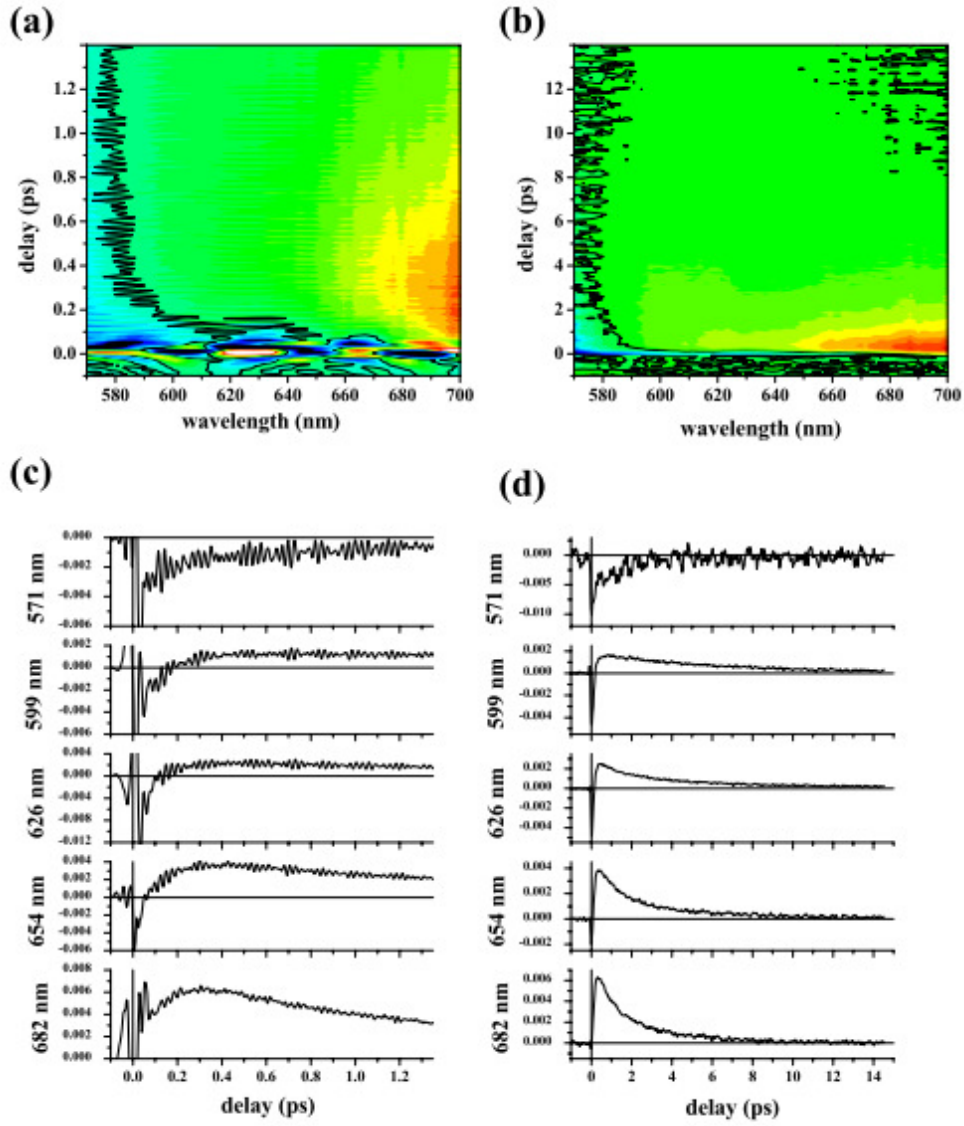


Figure 2: Measured 2D time-resolved absorbance difference spectra of DR19 in a solution sample (a) scanned from -0.1 to 1.4 ps and (b) that scanned from -1 to 14 ps. Black curves represent contours where the absorbance difference is zero ($\Delta A = 0$). (c), (d) Time-resolved ΔA traces at five different probe wavelengths picked up from (a) and (b), respectively.

ΔA is generally negative at probe wavelength below 580 nm. At these wavelengths, the ground state has an absorption band. Thus, ΔA is thought to be negative due to absorption bleaching, which implies that the electron population is depleted when DR19 is photoexcited by pump pulses. The positive ΔA observed at probe wavelengths longer than 580 nm was attributed to induced absorption of the excited state.

At first, we analyzed the exponential decays of the time traces to study the ultrafast dynamics of the electronic states during and after photoexcitation of DR19.

The ΔA traces in Figs. 2(c) and (d) contain three decay components with lifetimes of ~ 0.1 , ~ 1 , and ~ 10 ps. Therefore, the ΔA traces should be fitted by a triple exponential function given by

$$f(t, \lambda) = \Delta A_1(\lambda) e^{-\frac{t}{\tau_1}} + \Delta A_2(\lambda) e^{-\frac{t}{\tau_2}} + \Delta A_0(\lambda) e^{-\frac{t}{\tau_3}} \quad (\tau_1 < \tau_2 < \tau_3). \quad (1)$$

The τ_1 (~ 0.1 ps) lifetime component decays, becoming negligible at delay longer than 0.4 ps.

Therefore, we determined the other two time constants (τ_2 and τ_3) by fitting the ΔA trace in the long delay region between 0.4 and 14 ps using the following double exponential function

$$f(t, \lambda) = \Delta A_2(\lambda)e^{-\frac{t}{\tau_2}} + \Delta A_3(\lambda)e^{-\frac{t}{\tau_3}} \quad (\tau_2 < \tau_3). \quad (2)$$

Global fitting analysis estimated the time constants τ_2 and τ_3 to be 1.11 ± 0.13 and 4.65 ± 0.56 ps, respectively. Using the ΔA traces and the estimated time constants, the spectra of these lifetime components were calculated by the least-squares method (see Figs. 3).

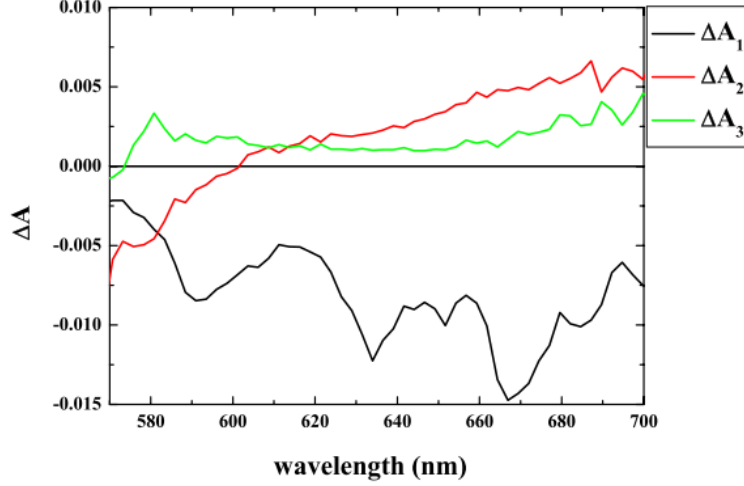


Figure 3: ΔA_1 , ΔA_2 , and ΔA_3 are spectral components of the DR19 solution sample, which decay with the lifetimes of τ_1 , τ_2 , and τ_2 , respectively.

The instrument response time of the present measurements was estimated to be 9 fs, which is considered negligible for delays longer than 50 fs. Therefore, we determined the shortest time constant (τ_1) and its spectral component (ΔA_1) by fitting the ΔA trace in the short delay region from 50 fs to 1.4 ps. In the fitting analysis, we applied the global fitting using the following double exponential function by fixing the parameter τ_2 to 1.11 ps (as estimated above). Note that the τ_3 -decay component can be considered constant for delays up to 1.4 ps. The function $f(t, \lambda)$ is given by

$$f(t, \lambda) = \Delta A_1(\lambda)e^{-\frac{t}{\tau_1}} + \Delta A_2(\lambda)e^{-\frac{t}{\tau_2}} + \Delta A_0(\lambda) \quad (\tau_1 < \tau_2), \quad (3)$$

where $\Delta A_0(\lambda)$ indicates a spectral component with an infinite lifetime. Global fitting analysis estimated the time constant τ_1 to be 104 ± 12 fs and its spectral component $\Delta A_1(\lambda)$ was obtained by the least-squares method (see Fig. 3).

The shortest time constant, τ_1 , had been only roughly estimated in previous studies because of their limited time resolutions. In the present study using a 9 fs pulse, τ_1 was accurately estimated to be 104 ± 12 fs. Its spectral component, $\Delta A_1(\lambda)$, does not reflect the spectral profile of the stationary absorption spectrum shown in Fig. 1. Therefore, the shortest decay component does not include decay to the electronic ground state and it was attributed to large amplitude wave-packet motion on the excited-state potential surface out of the Franck-Condon (FC) region [21]. The negative spectrum of ΔA_1 is considered to be the stimulated emission spectrum of the FC state.

The time constant τ_2 was estimated to be 1.11 ± 0.13 ps. Its spectral component, $\Delta A_2(\lambda)$, is

negative, reflecting the spectral profile of the stationary absorption spectrum at probe wavelengths shorter than 580 nm. Therefore, the wave packet generated by the photoexcitation is considered to be spread over the potential energy surface of the electronic excited state and to locate the conical intersection to the ground state via photo-isomerization around the NN double bond; this process is responsible for the time constant of τ_2 [22]. When probe wavelength is longer than 620 nm, $\Delta A_2(\lambda)$ is positive and induced absorption is the dominant process.

The time constant τ_3 was determined to be 5.86 ± 2.13 ps. Its spectral component, $\Delta A_3(\lambda)$, has a flat profile with a positive value reflecting induced absorption. Koller et al. [10] elucidated that vibrational cooling in the ground state occurs in 4-nitro-40-(dimethylamino)azobenzene with a time constant of 5.5 ps. Therefore, τ_3 is assigned to the vibrational cooling time in the ground state of DR19.

Next, we have analyzed the oscillation observed in the time traces shown in Figs. 2(c) and (d). The periodic oscillations reflect molecular vibrations that occur during the reaction after photoexcitation; these oscillations have been theoretically studied [23] and observed in various experiments [19,24,25]. Fourier transform of the time trace measured at 626 nm (see Fig. 4(a)) was calculated as shown in Fig. 4(b). It agrees with Raman spectrum [26], confirming that the oscillations in the time-resolved trace are caused by molecular vibrations.

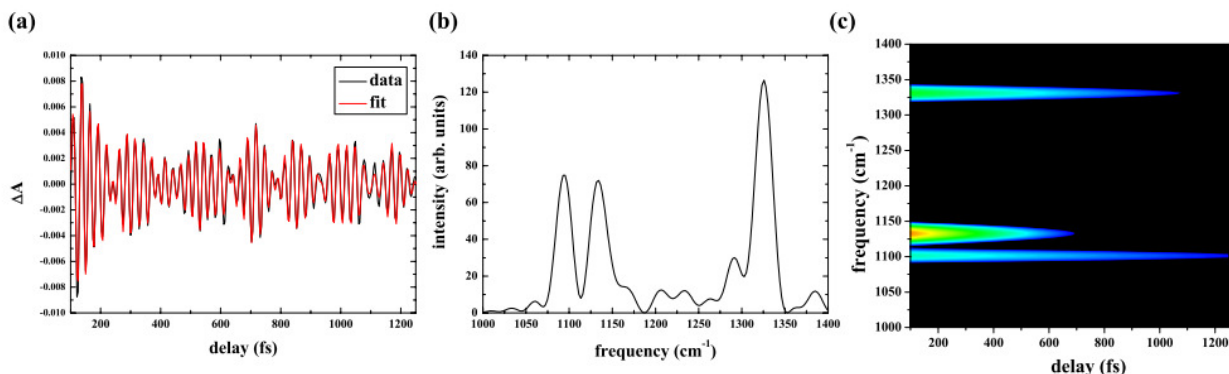


Figure 4: (a) The time trace of DR19 in solution measured at 626 nm (black curves) and the time trace reconstructed in LP-SVD analysis (red curves). (b) Fourier power spectrum of the measured time trace shown in (a). (c) Two dimensional view of the intensity of the vibrational modes obtained in the LP-SVD analysis.

The vibrational dynamics was analyzed using linear prediction and singular value decomposition (LP-SVD) [27-29]. Table 1 shows the frequencies, amplitudes, and lifetimes of the vibrational modes obtained in the LP-SVD analysis. The obtained parameters are also shown as a two dimensional view in Fig. 4(c). Using the obtained parameters, the time trace was reconstructed as shown in Fig. 4(a) agreeing with the measured time trace. The vibration modes of 1100, 1131, and 1330 cm^{-1} are assigned to ϕ -N stretching, C-H deformation, NO_2 symmetric stretching modes, respectively, referring the Raman study [26]. The result of the LP-SVD analysis shows that the C-H deformation has distinctly high amplitude and fast lifetime among these three vibration modes. It reflects that photo-isomerization of the DR19 in solution causes large deformation around the C-H bond in its primary process.

Table 1: Results obtained in the LP-SVD analysis for DR19 in solution.

frequency (cm^{-1})	amplitude	decay (fs)
1100	107	2510
1131	285	458
1330	141	1411

3.2 Comparison with ultrafast dynamics of the film sample

Figure 5(a) shows two-dimensional plot of the ΔA spectrum of the DR19 film sample measured for delays from -0.1 to 1.4 ps (short delay region) and probe wavelengths from 514 to 758 nm. Figure 5(b) shows the ΔA spectrum measured between -1 and 14 ps (long delay region) in the same probe wavelength region. The black curves in Figs. 5(a) and (b) are contours for which ΔA is zero. Figures 5(c) and (d) show ΔA traces at five different probe wavelengths in Figs. 5(a) and (b).

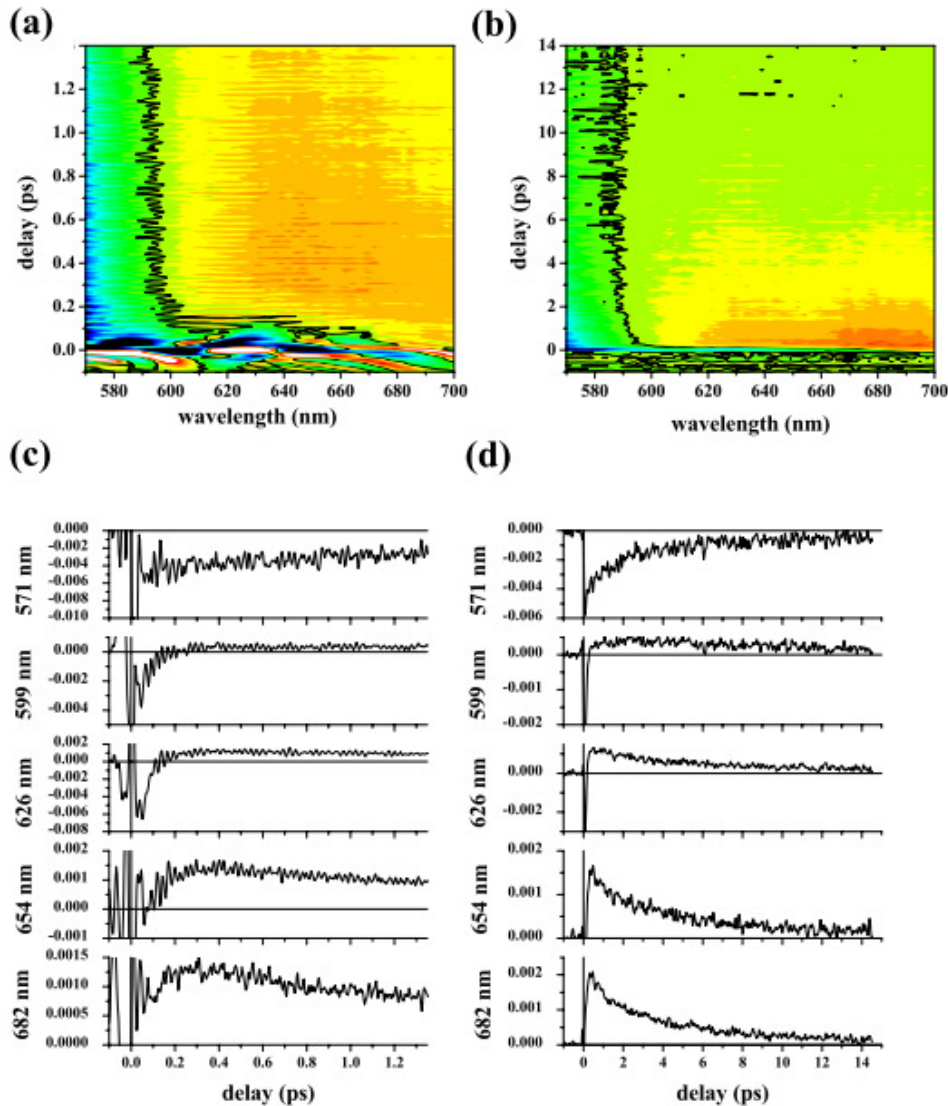


Figure 5: Measured 2D time-resolved absorbance difference spectra of DR19 in a film sample (a) scanned from -0.1 to 1.4 ps and (b) that scanned from -1 to 14 ps. Black curves represent contours where the absorbance change is zero ($\Delta A = 0$). (c), (d) Time-resolved ΔA traces at five typical probe wavelengths picked up from (a) and (b), respectively.

Similar to the solution sample, the negative ΔA at delays shorter than 580 nm is assigned to absorption bleaching caused by depletion of the ground state and the positive ΔA observed at probe wavelengths longer than 580 nm reflects induced absorption of the excited state.

The ΔA traces of the film sample in Figs. 5(c) and (d) also include three decay components with lifetimes of ~ 0.1 , ~ 1 , and ~ 10 ps. Therefore, the ΔA traces were fitted in the same manner as the traces of the solution sample.

We first fitted the ΔA trace in the long delay region using Eq. (2) for delays from 0.4 ps to 14 ps. Global fitting analysis estimated the time constants of τ_2 and τ_3 to be 1.35 ± 0.19 and 5.77 ± 0.81 ps, respectively. The spectral components of the obtained time constants were obtained by the least-squares method (see Fig. 6).

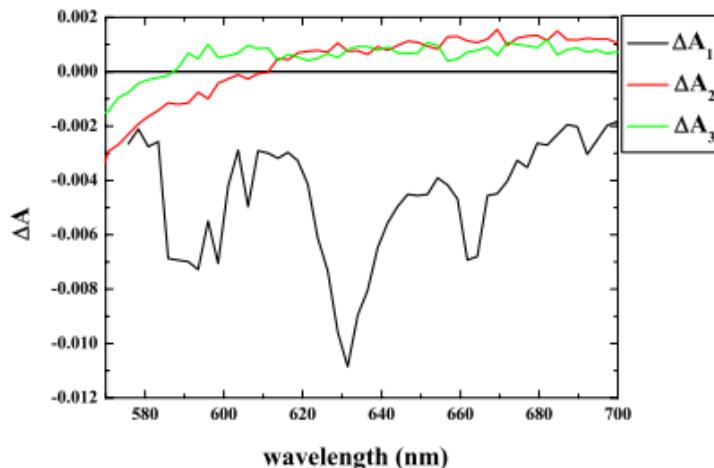


Figure 6: ΔA_1 , ΔA_2 , and ΔA_3 are spectral components of the DR19 film sample, which decay with the lifetimes of τ_1 , τ_2 , and τ_2 , respectively.

Compared with this data for DR19 in the film sample, ΔA_2 has large positive amplitude in the wavelength region reflecting existence of induced absorption longer than 620 nm in solution (see Fig. 3). The reason why the induced absorption appears in the solution sample of DR19 is thought to be explained as follows. The DR19 has a push-pull substituted structure with a large dipole moment of 8 Debye, and the solvent of TMTE is a polar solvent with a dipole moment of 3 Debye. Therefore, there is a strong dipole interaction between the DR19 and the solvent in the solution sample. The strong interaction modifies the electronic states of the higher excited state, which opens a way for the induced absorption via transition from the first excited state to the higher excited state.

The shortest time constant (τ_1) and its spectral component (ΔA_1) were then estimated by fitting the ΔA trace in the short delay region from 50 fs to 1.4 ps. Global fitting of the ΔA traces using Eq. (3) estimated the time constant τ_1 to be 74 ± 10 fs. The spectral component of τ_1 ($\Delta A_1(\lambda)$) was obtained by the least-squares method and is plotted in Fig. 6.

The shortest time constant, τ_1 , was estimated to be 74 ± 10 fs. For the same reason given above for the solution sample, the shortest decay component was attributed to a large amplitude wave-packet motion on the excited-state potential surface out of the FC region. The negative spectrum of ΔA_1 was considered to be the stimulated emission spectrum of the FC state. DR19 is

known to have a large dipole moment of up to 8 Debye [12,13] because of its push-pull substituted structure. Therefore, photoexcitation of DR19 generates a charge-transfer (CT) state via electron transfer. Inter- and intramolecular modes adapt within τ_1 to the new charge distribution generated by CT excitation. The solution and film samples had similar shortest time constant τ_1 , which implies that solutions and films of DR19 have comparable adaptation speeds.

The time constant τ_2 is estimated to be 1.35 ± 0.19 ps. $\Delta A_2(\lambda)$ is negative at wavelength below 610 nm reflecting the spectral profile of the stationary absorption spectrum. Therefore, τ_2 in the film sample was also assigned to the time for the photoexcited wave packet in the excited state to find the conical intersection to the ground state via photo-isomerization around the NN double bond; this process is responsible for the time constant τ_2 . When probe wavelength is longer than 610 nm, $\Delta A_2(\lambda)$ is positive and induced absorption is the dominated process.

The time constant of τ_3 was determined to be 5.77 ± 0.81 ps. Its spectral component, $\Delta A_3(\lambda)$, has a flat profile with a positive induced absorption. Just as for the solution sample, τ_3 reflects the vibrational cooling time in the ground electronic state of DR19.

Fourier transform of the time trace measured at 626 nm (see Fig. 7(a)) was also calculated for DR19 in a film sample as shown in Fig. 7(b). It agrees with the result obtained for solution sample (see Fig. 4(b)) and Raman spectrum [26]. The LP-SVD analysis was performed for the time trace of the film sample. Table 2 shows the frequencies, amplitudes, and lifetimes of the vibrational modes obtained in the LP-SVD analysis. The obtained parameters are also shown as a two dimensional view in Fig. 7(c). Using the obtained parameters, the time trace was reconstructed as shown in Fig. 7(a) agreeing with the measured time trace. The assignments of 1099, 1126, and 1324 cm^{-1} are same as those of the solution sample assigned to ϕ -N stretching, C-H deformation, NO_2 symmetric stretching modes, respectively, referring the Raman study [26]. The result of the LP-SVD analysis shows that all of those three modes have similar amplitude and fast lifetime of ~ 500 fs. It reflects that photo-isomerization of the DR19 in the film sample causes structural deformation equally among ϕ -N bond, C-H bond, and NO_2 group. The result is significantly different from that of the DR19 in solution, which only the C-H deformation was dominantly excited. It is thought to be that the strong dipole interaction between TMTE and DR19 in the solution sample suppresses deformations along the dipole moment of the DR19 only allowing the C-H deformation.

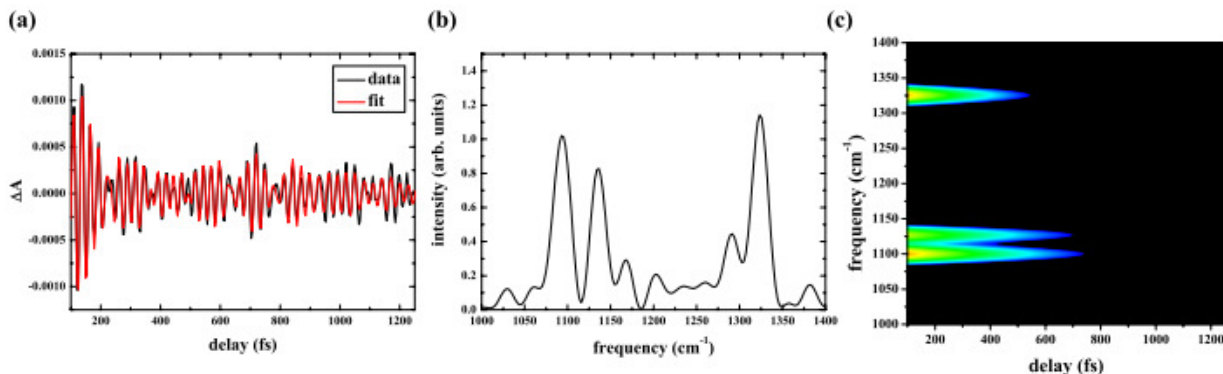


Figure 7: (a) The time trace of DR19 in a film sample measured at 626 nm (black curves) and the time trace reconstructed in LP-SVD analysis (red curves). (b) Fourier power spectrum of the measured time trace shown in (a). (c) Two dimensional view of the intensity of the vibrational modes obtained in the LP-SVD analysis.

Table 2: Results obtained in the LP-SVD analysis for DR19 in a film sample.

frequency (cm^{-1})	amplitude	decay (fs)
1099	35	518
1126	27	588
1324	36	369

4. Summary

The photoisomerization of DR19 in solution and a polymer film were investigated absorbance difference measurements over a broadband visible spectral range and with a time resolution of 9 fs. The DR19 has a push-pull substituted structure, which forms the CT state via electron transfer after photoexcitation. Therefore, the film sample may have different dynamics from the solution sample because significant intermolecular CT in the film modifies the relaxation pathway of the CT state. The observed time traces contain three decay components with lifetimes of ~ 0.1 , ~ 1 , and ~ 10 ps. We estimated the three time constants (τ_1 , τ_2 , and τ_3) and their spectral components (ΔA_1 , ΔA_2 , and ΔA_3) by fitting the time-resolved ΔA trace with a triple exponential function.

The shortest time constant, τ_1 , had been roughly estimated in previous studies. In this study, τ_1 was precisely estimated for both the solution sample (104 ± 12 fs) and film (74 ± 10 fs) samples. Its spectral component, ΔA_1 , is negative, reflecting stimulated emission from the FC state. The τ_1 decay component was attributed to a large amplitude wave-packet motion on the excited-state potential surface out of the FC region.

The spectral component, $\Delta A_2(\lambda)$, is negative reflecting the spectral profile of the stationary absorption spectrum for probe wavelengths shorter than 580 nm. This implies that the wave packet generated by the photoexcitation is spread over the potential energy surface of the electronic excited state and finds the conical intersection to the ground state via photo-isomerization around the NN double bond; this process is responsible for the time constant of τ_2 .

The longest spectral component, $\Delta A_3(\lambda)$, has a flat profile and is positive due to induced absorption. Its time constant, τ_3 , is much longer than τ_2 reflecting the vibrational cooling time in

the ground electronic state of DR19.

In the present study, we clarified the ultrafast dynamics of a push-pull substituted azobenzene dye, DR19, which is known to have a large dipole moment and is promising for various applications. Ultrafast time-resolved absorbance difference spectroscopy is expected to provide essential information for photonic applications and is a promising alternative method for evaluating switching performance.

(2) 參考文獻

After we developed the fastscan ultrafast spectroscopy system, we have published the result in the peer-reviewed journal, Review of Scientific Instruments [1]. Our results demonstrated that the **signal quality was dramatically improved** by using the newly developed system. We have been applying the system for the study of ultrafast dynamics of various materials.

The newly developed system was applied for ultrafast spectroscopy of photo-voltaic polymer, P3HT, and the result was published in a peer-reviewed scientific journal of Chemical Physics Letters [2]. Using the fastscan ultrafast spectroscopy system, we could get signal of the P3HT film with high signal-to-noise ratio, and estimated the time constant of the relaxation dynamics of bound polaron on the P3HT polymer chains. The results were also well summarized in a doctor thesis of Dr. Yu-Hsien Lee [3].

Another application for ultrafast spectroscopy was performed for Azo dye, DR19 (to be published on a peer-reviewed journal, The Journal of Physical Chemistry A [4]. The dynamics of the DR19 film is hard to be observed because the film can be easily damaged by photo irradiation. The fastscan ultrafast spectroscopy system allowed us to study the ultrafast dynamics of the film because the effect of the photo damage is negligible in each scan of the fast scan finishing in five seconds. Preliminary result of ultrafast spectroscopy of this material was reported on a master thesis of Ms. Chun-Chih Hsu [5].

We have been working on ultrafast spectroscopy of various materials using traditional system of ultrafast spectroscopy in parallel with above development of the fastscan ultrafast spectroscopy system [6-20]. The stepscan stage used for the traditional ultrafast spectroscopy system was moved to the quantum information experiment system, and we developed and demonstrated two new schemes to generate entangled photon pairs applying our knowledge on time-resolved spectroscopy. Each of the results on two schemes was published on a peer-reviewed journal of Phys. Rev. A [21,22]. These results were summarized in a Ph. D. thesis of Dr. Hsin-Pin Lo [23].

References

- [1] "Development of a multiplex fast-scan system for ultrafast time-resolved spectroscopy", Atsushi Yabushita, Yu-Hsien Lee, and Takayoshi Kobayashi, Rev. Sci. Instr., 81, 063110 (2010)
- [2] "Ultrafast relaxation dynamics of photoexcitations in poly(3-hexylthiophene) for the determination of the defect concentration", Yu-Hsien Lee, Atsushi Yabushita, Chain Shu Hsu, Sheng Hsiung Yang, Izumi Iwakura, Chih Wei Luo, Kaung Hsiung Wu, Takayoshi Kobayashi, Chem. Phys. Lett., 498, 71-76 (2010)
- [3] Yu-Hsien Lee (2011) Development of NOPA System for Study of Ultrafast Dynamics, unpublished thesis (Ph. D.), National Chiao-Tung University.
- [4] "Environment-Dependent Ultrafast Photoisomeriation Dynamics in Azo Dye",

- Chun-Chih Hsu, Yu-Ting Wang, Atsushi Yabushita, Chih-Wei Luo, Yi-Nan Hsiao, Shiuan-Huei Lin, and Takayoshi Kobayashi, *The Journal of Physical Chemistry A*, dx.doi.org/10.1021/jp2051307, to be published (2011).
- [5] Chun-Chih Hsu (2009) Ultrafast photoisomerization dynamics of azo dye in solution and a polymer film, unpublished thesis (M. S.), National Chiao-Tung University.
- [6] "Novel reversible chemosensory material based on conjugated side-chain polymer containing fluorescent pyridyl receptor pendants", H.C. Chu, Y.H. Lee, S.J. Hsu, P.J. Yang, A. Yabushita, H.C. Lin, *J. Phys. Chem. B*, 115, 8845-8852 (2011).
- [7] "Ultrafast electronic and vibrational dynamics of a ruthenium porphyrin complex in intersystem crossing", T. Kobayashi, I. Iwakura, A. Yabushita, *Physics Procedia*, 13, 24-27 (2011)
- [8] "Ultrafast dynamics of excited state in oxy-hemoglobin", T. Kobayashi, A. Yabushita, *Chinese Optics Letters*, 9, S10605 (2011)
- [9] "Spectral phase retrieval of 8 fs optical pulses at 600nm by using a collinear autocorrelator with 300um-thick lithium triborate crystals", C.S. Hsu, Y.H. Lee, A. Yabushita, T. Kobayashi, S.D. Yang, *Opt. Lett.*, 36, 2041-2043 (2011).
- [10] "Transition-state spectroscopy using ultrashort laser pulses", T. Kobayashi, and A. Yabushita, *Chem. Rec.*, 11, 99-116 (2011).
- [11] "Transition state in a prevented proton transfer observed in real time", Izumi Iwakura, Atsushi Yabushita, Takayoshi Kobayashi, *Bull. Chem. Soc. Jpn.*, 84, 2, 164-171 (2011)
- [12] "Non-thermal reaction triggered by a stimulated Raman process using 5-fs laser pulses in the electronic ground state: Claisen rearrangement of allyl phenyl ether", Izumi Iwakura, Atsushi Yabushita, and Takayoshi Kobayashi, *Chem. Phys. Lett.*, 501, 567-571 (2011)
- [13] "Ultrafast dynamics in optimally doped YBa₂Cu₃O_{7-δ} observed with white light pump-probe spectroscopy", Y.T. Wang, Y.H. Lee, Y.J. Chen., W.T. Tang, C.W. Luo, A. Yabushita, K.H. Wu., J.Y. Lin, J.Y. Juang, T.M. Uen, T. Kobayashi, *J. Sup. Nov. Mag.*, 24, 519-521 (2011).
- [14] "Beat of frequency modes with an artificial negative frequency in spectrogram analysis", Atsushi Yabushita, Chih-Hsien Kao, Yu-Hsien Lee, Takayoshi Kobayashi, *Chem. Lett.*, 39, 1283-1284 (2010)
- [15] "Kinetic isotope effect on the proton-transfer in indigo carmine Directly Observed by Real-time Vibrational Spectroscopy Few-cycle pulse Laser", T. Kobayashi, I. Iwakura and A. Yabushita, *ISOTOPES 2011*, 41 (2011)
- [16] "Polarization entangled beam-like photon pairs generated by spontaneous parametric down conversion", T. Kobayashi, H.-P. Lo, P.-C. Chen, C.-W. Luo, A. Yabushita, 8th International Symposium on Modern Optics and Its Applications (ISMOA), 49-50 (2011)

- [17] "Ultrafast spectroscopy of oxyhemoglobin during photodissociation", Atsushi Yabushita and Takayoshi Kobayashi, *J. Phys. Chem. B*, 114, 11654-11658 (2010)
- [18] "Primary events in the photodissociation of oxyhemoglobin", Atsushi Yabushita and Takayoshi Kobayashi, *Spectroscopy*, 24, 333-338 (2010)
- [19] "Direct observation of the molecular structural changes during the Claisen rearrangement including the transition state", Izumi Iwakura, Atsushi Yabushita, and Takayoshi Kobayashi, *Chem. Lett.*, 39, 374-375 (2010)
- [20] "Vibrational fine structures revealed by the frequency-to-time fourier transform of the transient spectrum in bacteriorhodopsin", Atsushi Yabushita and Takayoshi Kobayashi, *J. Phys. Chem. B*, 114, 4632-4636 (2010)
- [21] "Kinetic isotope effect on the proton-transfer in indigo carmine", Izumi Iwakura, Atsushi Yabushita, Takayoshi Kobayashi, *Chem. Phys. Lett.*, 484, 4-6, 354-357 (2010)
- [22] "Solvent effect for ruthenium porphyrin", Izumi Iwakura, Atsushi Yabushita, and Takayoshi Kobayashi, *Science China*, 53, 6, 1005-1012 (2010)
- [23] "Direct observation of molecular structural change during intersystem crossing by real-time spectroscopy with a few optical cycle laser", T. Kobayashi, I. Iwakura, and A. Yabushita, Program proceeding for ACUP 2010, 136 (2010)
- [24] "Relaxation dynamics of bounded polaron pairs in polythiophene derivative", Y. H. Lee, A. Yabushita, C. S. Hsu, S. H. Yang, C. W. Luo, K. H Wu, and T. Kobayashi, Program proceeding for ACUP 2010, 142 (2010)
- [25] "Time-resolved spectroscopy of photo-dissociation process of oxy-hemoglobin", A. Yabushita and T. Kobayashi, The 1st Ultrafast Dynamics Symposium, 26 (2010)
- [26] "Relaxation dynamics of bounded polaron pairs in polythiophene derivative", Y. H. Lee, A. Yabushita, C. S. Hsu, S. H. Yang, C. W. Luo, K. H Wu, and T. Kobayashi, The 1st Ultrafast Dynamics Symposium, 24 (2010)
- [27] "Why is Indigo Photostable over Extremely Long Periods?", Izumi Iwakura, Atsushi Yabushita, Takayoshi Kobayashi, *Chem. Lett.*, 38, 11, 1020-1021 (2009)
- [28] "Dynamics of vibrational and electronic coherences in the electronic excited state studied in a negative-time range", Takayoshi Kobayashi and Atsushi Yabushita, *Chem. Phys. Lett.*, 482, 1-3, 143-147 (2009)
- [29] "Direct observation of molecular structural change during intersystem crossing by real-time spectroscopy with a few optical cycle laser", Izumi Iwakura, Takayoshi Kobayashi, and Atsushi Yabushita, *Inorg. Chem.* 48, 3523-3528 (2009)
- [30] "Primary conformation change in bacteriorhodopsin on photoexcitation", Atsushi Yabushita and Takayoshi Kobayashi, *Biophys. J.* 96, 1447-1461 (2009)
- [31] "Parametric interaction and nonlinear Raman processes of vibronic excitons in polydiacetylene studied with a two-optical-cycle laser", Takayoshi Kobayashi, Izumi Iwakura, and Atsushi Yabushita, *Phys. Stat. Sol. C*, 6, 152-155 (2009)
- [32] "Transition states and nonlinear excitation in chloroform observed with a sub-5 fs pulse laser", Izumi Iwakura, Atsushi Yabushita, and Takayoshi Kobayashi, *J.*


- Am. Soc. Chem., 131, 688-696 (2009)
- [33] "Real-time observation of the bond length modulation of carbon double bond during the photoisomerization of bacteriorhodopsin", T. Kobayashi and A. Yabushita, *Ultrafast Phenomena XVI*, 568-570 (2009)
- [34] "Excitonic and vibrational nonlinear process in a polydiacetylene studied by a few-cycle pulse laser", T. Kobayashi, I. Izumi, and A. Yabushita, *Phys. Stat. Sol. C*, 6, 1, 16 (2009)
- [35] "Direct observation of molecular structural change during intersystem crossing by real-time spectroscopy with a few optical cycle laser", T. Kobayashi, I. Iwakura, and A. Yabushita, *Femtochemistry IX*, 35 (2009)
- [36] Chih-Hsien Kao (2011) Ultrafast time-resolved study of CIGS films, unpublished thesis (M. S.), National Chiao-Tung University.
- [37] "Beamlike photon pairs entangled by a 2x2 fiber", H.P. Lo, A. Yabushita, C.W. Luo, P.C. Chen, T. Kobayashi, *Phys. Rev. A*, 84, 022301 (2011)
- [38] "Beamlike photon-pair generation for two-photon interference and polarization entanglement", Hsin-Pin Lo, Atsushi Yabushita, Chih-Wei Luo, Pochung, Chen, Takayoshi Kobayashi, *Phys. Rev. A*, 83, 022343 (2011).
- [39] Hsin-Pin Lo (2011) Generation and studies of beamlike polarization-entangled photon pair, unpublished thesis (Ph. D.), National Tsing Hua University.

(3) 計畫成果自評

As a result of this project, I have finished the development of the fast scan system as I planned in the project proposal. **The result of fast scan system development has been published** as an article in a peer-reviewed scientific journal of "Review of Scientific Instruments". The title of the article is "Development of a multiplex fast-scan system for ultrafast time-resolved spectroscopy" written by Atsushi Yabushita, Yu-Hsien Lee, and Takayoshi Kobayashi. The article was printed in Volume 81, Issue 7 of the journal in 2010. **I have successfully accomplished the development of the fastscan ultrafast spectroscopy system, which was planned to be done in the first and second year of this project.**

target (1st and 2nd year)
Development of fastscan ultrafast spectroscopy system

Mission completed!!
each of scan can finish just in 5 seconds

 **solved problems!**

- ~~❌ damage accumulation on sample~~
- ~~❌ long-term instability (~minutes) of light source~~

Excellent improvements in

- ✅ signal-to-noise ratio
- ✅ reproducibility (reliability) of the signal

In the third year of this project, I was planning to apply the developed system for study of ultrafast dynamics. Actually, I have used the newly developed system to study the following two materials and **confirmed that the system is really a powerful tool to study ultrafast dynamics** of various materials improving the signal-to-noise ratio of the time-resolved signals..

The newly developed system was applied for ultrafast spectroscopy of photo-voltaic polymer, P3HT, and **the result was published** in a peer-reviewed scientific journal of Chemical Physics Letters (Yu Hsien Lee et al, "Ultrafast relaxation dynamics of photoexcitations in poly(3-hexylthiophene) for the determination of the defect concentration", Chem. Phys. Lett. 398, 71-76 (2010)). Using the fastscan ultrafast spectroscopy system, we could get signal of the P3HT film with high signal-to-noise ratio, and estimated the time constant of the relaxation dynamics of bound polaron on the P3HT polymer chains

We also performed ultrafast spectroscopy of Azo dye, DR19, and **the result was accepted for publication** on a peer-reviewed journal (Chun-Chih Hsu et al, "Environment-Dependent Ultrafast Photoisomerization Dynamics in Azo Dye", The Journal of Physical Chemistry A,

dx.doi.org/10.1021/jp2051307, to be published). The dynamics of the DR19 film is hard to be observed because the film can be easily damaged by photo irradiation. The fastscan ultrafast spectroscopy system allowed us to study the ultrafast dynamics of the film because the effect of the photo damage is negligible in each scan of the fast scan finishing in five seconds.

target (3rd year)

Application of fastscan ultrafast spectroscopy system

**We applied the system to study various materials
confirming that it is really powerful**

- ✔ P3HT (for polymer solar cell)
published on Chemical Physics Letters
- ✔ azoaromatic dye (for hologram, etc)
accepted for publication on the Journal of Physical Chemistry A

The accomplishment of the development of the fastscan ultrafast spectroscopy system and its successful applications show that this project was **accomplished successfully in 100%**.

Summary

研究內容與原計畫相符程度

I was planning to develop a fastscan ultrafast spectroscopy system. As I have expected, the newly developed system works well to improve signal quality. I have **performed the project exactly as I have planned** in the project proposal.

達成預期目標情況

1st year Data acquisition (DAQ) system should store data in memory at the timing when it receives external trigger signal. I **finished the development of the software** for the data acquisition in the first year **on time**.

2nd year Fastscan spectroscopy need to synchronize the DAQ timing with the fast scan stage. In the 2nd year, we have **accomplished** the synchronization and the development of the fastscan spectroscopy system **on time**.

3rd year The system developed until 2nd year of this project was applied for ultrafast spectroscopy of various materials. The data obtained by the system shows **quite high quality beyond our expectation**.

研究成果之學術或應用價值

The system developed in this project improves signal quality of ultrafast spectroscopy and allows us to study various materials even for photofragile materials. It means that our system is **a key technology in the ultrafast spectroscopy**, and our collaborator is also starting to be used this methodology in Japan.

是否適合在學術期刊發表或申請專利

The system development was already published in Review of Scientific Instruments. **As application of the system**, we have studied several materials and **published as papers** reporting each of those results, respectively.

主要發現或其他有關價值等

In this project, we developed a quite useful instrument for ultrafast spectroscopy and found that the system can observe ultrafast dynamics of various materials even for photofragile materials avoiding photo-damage. Until the development of this system, we had difficulty in ultrafast spectroscopy of biomaterials. **The fastscan ultrafast spectroscopy system becomes a breakthrough to solve the difficulties in ultrafast spectroscopy**.